LITHOS 432–433 (2022) 106894

Contents lists available at ScienceDirect

LITHOS

journal homepage: www.elsevier.com/locate/lithos

Mineralogy and geochemistry of serpentinized peridotites of the Northern Nubian Shield: The origin of compositionally banded olivine and implications for Neoproterozoic supra-subduction zone metasomatism

Mohamad A. Ismail [a], Ayman E. Maurice [a,*], Paul D. Asimow [b], Moustafa E. Gharib [a,1], M.J. Wilner [b], Hussam A. Selim [a]

[a] Geology Department, Faculty of Science, Helwan University, 11790 Cairo, Egypt
[b] Division of Geological and Planetary Sciences, California Institute of Technology, Pasadena, CA 91125, USA

ARTICLE INFO

Keywords:
Neoproterozoic ophiolite
Fore-arc peridotite
Serpentinite
Metasomatism
Banded zoning
Eastern Desert

ABSTRACT

A sequence of Neoproterozoic ultramafic rocks — serpentinized peridotite, serpentinite, and clinopyroxenite — outcrop in Wadi El-Mireiwa in the south Eastern Desert of Egypt. They represent the mantle and lowermost crustal section of a fragmented ophiolite, emplaced by thrusting above metasedimentary rocks and an island arc assemblage and later intruded by a granite mass. In samples of the serpentinized peridotite, back-scattered electron images of olivine reveal banded zoning, defined by straight and parallel Mg-enriched (Fo ~ 96) lamellae within typically magnesian host crystals (Fo ~ 89). The presence of clinopyroxene, the relatively low whole-rock Mg# (~88), the low NiO content of olivine (0.1–0.32 wt%), and the relatively high TiO_2 content of fresh Cr-spinel (~0.3 wt%) are all consistent with a cumulate origin for the serpentinized peridotite and serpentinites. On the other hand, some associated serpentinite has higher whole-rock Mg# (92) and low TiO_2 in Cr-spinel (~0.01 wt%), consistent with a residual origin by high-degree melt extraction in the fore-arc region of a supra-subduction zone (SSZ) environment. The formation of Mg-enriched bands in olivine is attributed to the enhancement of metasomatic Mg-Fe exchange with high-Mg/Fe^{2+} fluids along crystallographically-oriented subgrain boundaries produced by high strain-rate dislocation creep. Such high-Mg/Fe^{2+} fluid metasomatism also explains reverse zoning of MgO in Cr-spinel, whereas the low whole-rock concentrations of REE and other trace elements exclude a significant role for melt-rock interaction. The evidence for high-Mg/Fe^{2+} fluid metasomatism in this suite indicates that SSZ fluids and high fore-arc strain rates affect not only the mantle wedge but also overlying ultramafic cumulates. The oxygen fugacity [$\Delta \log fO_2$(FMQ)] values calculated from unmetasomatized (+2.48 to +2.67) and metasomatized (+3.75 to +4.53) samples reflect the oxidized nature of Neoproterozoic SSZ magma and the even more oxidizing character of the metasomatic fluids. Banded zoning has also been recorded in olivine from Mariana fore-arc peridotite and Phanerozoic SSZ ophiolites; the Neoproterozoic Wadi El-Mireiwa case shows that rapid mantle flow has been a persistent feature of the tectonic environment where fore-arc ophiolites develop.

1. Introduction

Peridotites — i.e., olivine-dominant ultramafic rocks — are found in a variety of tectonic settings, including plate margins of all varieties as well as intra-plate locations (e.g., DeBari and Coleman, 1989). They may be exposed, often tectonized, fragments of the mantle or they may be lower crustal magmatic rocks, often as members of layered or other mafic-ultramafic intrusions. Although mantle and magmatic peridotites have similar mineral constituents, they differ in texture, mineral compositions, and whole-rock chemistry (e.g., Arai, 1994; Hébert and Laurent, 1989). Hence the compositions of primary minerals — including olivine, spinels, and pyroxenes — are often used to infer the tectonic setting, petrogenesis and evolution of peridotites (e.g., Ali et al., 2020; Arai, 1994; Dick and Bullen, 1984; Kamenetsky et al., 2001; Maurice et al., 2021), supplemented by constraints from whole-rock trace element contents. The mineral chemistry of both mantle-derived and

* Corresponding author.
E-mail address: Ayman.Maurice@science.helwan.edu.eg (A.E. Maurice).
[1] Deceased.

https://doi.org/10.1016/j.lithos.2022.106894
Received 10 June 2022; Received in revised form 18 September 2022; Accepted 24 September 2022
Available online 30 September 2022

magmatic peridotites can be used, for example, to infer the oxidation state of magmatic systems, which become increasingly oxidized from mid-ocean ridge to subduction-influenced settings (Cottrell et al., 2021). On the other hand, peridotites have generally experienced alteration, metamorphism, and metasomatism that can partly or completely overprint their primary magmatic character. Gamal El Dien et al. (2019), for example, proposed that the composition of Cr-spinel in supra-subduction zone peridotites is more useful as a tracer of metasomatic processes than as a geotectonic or mantle melting indicator.

Ophiolite sequences with well-developed ultramafic mantle sections are widely distributed in the central and southern sectors of the Eastern Desert of Egypt, which represents the northwestern tip of the Neoproterozoic Arabian-Nubian Shield. They represent relics of the lithosphere of the Mozambique Ocean that once separated East and West Gondwana. Although complete ophiolite sections are recorded in a few areas (e.g., the Fawakhir, Ghadir and Gerf Ophiolites; El-Sharkawy and El-Bayoumi, 1979; Abd El-Rahman et al., 2009; Basta et al., 2011; Abdel-Karim et al., 2016), the majority of Egyptian ophiolites are dismembered and lack one or more of the characteristic lithologies. The ultramafic sections of the Eastern Desert ophiolites are dominated by harzburgite and dunite (e.g., Ali et al., 2020), with rare cumulate wehrlite (e.g., Gahlan et al., 2015) and local podiform chromitite (e.g., Ali et al., 2020). The Eastern Desert ophiolites are Neoproterozoic in age; although traditionally thought to be older than 730 Ma (Maurice et al., 2021 and references therein), some recent work has yielded younger ages from 698 to 720 Ma (Zoheir et al., 2022). Although all the tectonic settings where ophiolites might develop — including mid-ocean ridge (e.g., El-Sharkawy and El-Bayoumi, 1979), back-arc (e.g., Basta et al., 2011) and fore-arc (e.g., Azer and Stern, 2007) settings — have been proposed for the Eastern Desert ophiolites, recent reviews have concluded that they are dominated by the fore-arc supra-subduction zone setting (Shahien et al., 2021).

In supra-subduction zone environments, there are large fluxes of slab-derived fluids that transport fluid-mobile elements and can be associated, depending on conditions, with both serpentinization (hydration of primary olivine) and deserpentinization (producing secondary olivine) (Clarke et al., 2020). Olivine serpentinization in subduction zones results in recycling of hydrogen to the mantle and production of abiotic methane (e.g., Boutier et al., 2021). In addition, metamorphic olivine plays an important role in recycling of elements to the deeper mantle; Kempf and Hermann (2018) proposed that incomplete dehydration of metamorphic olivine allows subducting slabs to transport water beyond the stability limits of nominally hydrous phases. In the Eastern Desert, the peridotites are all partly to completely serpentinized and many are further altered along shear zones and fault planes to form carbonate-bearing ultramafic rocks.

This study reports a new occurrence of banded zoning in olivine. Such banded zoning has previously been described in both mantle-derived and layered peridotites (e.g., Ando et al., 2001; Murata et al., 2009; Plümper et al., 2012). Banded olivine may be characterized by discrete stripes enriched either in Fe or in Mg relative to the bulk of the host olivine and these two types of banding may well have different origins. In both cases, their orientation is thought to be controlled by the organization of edge dislocations into subgrain boundaries during crystal-plastic olivine deformation under shear stress (Plümper et al., 2012). Mg-enriched stripes are thought to develop during antigorite serpentinization of olivine by enhanced diffusive exchange with metasomatic fluids along the subgrain boundary pathways (Plümper et al., 2012), whereas Fe-enriched stripes have been attributed to a mechanism (explained below) known as the Cottrell atmosphere (Ando et al., 2001). Because the pressure at which olivine transforms to fine-grained aggregates of the high-pressure polymorph wadsleyite decreases with increasing Fe content, Fe-rich bands have been invoked as a locus of superplastic grain-size sensitive flow that may trigger intermediate-focus earthquakes in the descending slab (Ando et al., 2001).

This study presents field, petrographic and geochemical investigations of a suite of Neoproterozoic ultramafic rocks in the Wadi El-Mireiwa area in the south Eastern Desert of Egypt, aiming to determine their nature (residual or magmatic) and tectonic setting. The association of banded olivine (recorded here for the first time, to our knowledge, in Neoproterozoic rocks) with reverse zoning in Cr-spinel provides an opportunity to evaluate the mechanism by which banded olivine developed in these rocks and to consider the implications for strain rate and metasomatism in the upper mantle above a Neoproterozoic subduction zone. Moreover, the coexistence, in the same serpentinized peridotite samples, of unmetasomatized Cr-spinel-olivine pairs and metasomatized zones of Cr-spinel in contact with olivine bands provides an opportunity to evaluate the oxidation state of a Neoproteroizoic SSZ mantle section and of the metasomatic fluids that fluxed through it.

2. Geological setting

The Wadi El-Mireiwa area is located in the northern part of the south Eastern Desert (SED) of Egypt (Fig. 1a). It occurs south of the Idfu-Mersa Alam Road, which follows an easterly direction and connects the Nile Valley with the Red Sea. The study area is located between latitudes 24° 49′ and 24° 56′ N and longitudes 34° 21′ and 34° 30′ E, covering an area of about 300 km^2 (Fig. 1b). The main Neoproterozoic map units in the area are metasedimentary rocks (metamudstone and metasiltstone), an ophiolite sequence, an island arc assemblage, and a younger granite intrusion. The ophiolite rocks have structural contacts against the metasedimentary and island arc sequences (Fig. 2a and b), interpreted as an overthrusting relationship. All these rock units are intruded by the younger granite (Fig. 2c). The metasedimentary rocks, dominantly pebbly metamudstone and metasiltstone, are considered to be the oldest unit in the study area. They preserve primary structures such as bedding and lamination defined by intercalation of lighter- and darker-toned beds.

The ophiolite sequence includes ultramafic rocks, metagabbro and metabasalt. The ophiolitic ultramafic rocks are moderately to highly serpentinized and crop out in two locations, Gebel El-Mireiwa and Gebel Mudargag El-Aswad. The ultramafic rocks of Gebel El-Mireiwa extend at least 18 km in an *E*-W direction and outcrop in two separated masses. The western mass forms an elongated ridge about 5.8 km long and 400 m wide. The smaller eastern mass extends for about 1.8 km, with an average width of 300 m. The ultramafic rocks of Gebel El-Mireiwa are medium to coarse-grained, varying in color from grayish black to dark black. They are mainly massive and include serpentinized peridotites (containing primary silicate relics), serpentinites (almost devoid of primary silicate relics) and serpentinized clinopyroxenites. In some outcrops, the ultramafic rocks are followed upwards by gabbros (Fig. 2d). The footwall metasediments beneath the ultramafic rocks of Gebel El-Mireiwa are squeezed and sheared due to thrusting. Scarce plagiogranite dykes and lenses are recorded cutting through the serpentinized ultramafic rocks of Gebel El-Mireiwa. The ultramafic rocks of Gebel Mudargag El-Aswad occur as an oval-shaped slab, about 150 m thick in the vertical direction, 900 m wide, and 2 km long. They are intruded by pink biotite granite of Gebel Mudargag El-Ahmer with a sharp contact between the two rock units (see Fig. 2c). Away from the contact zone, the ultramafic rocks are fine- to medium-grained massive rocks varying in color from dark black to grey, whereas the contact zone features highly sheared, schistose, grayish or yellowish-brown exposures. Locally, the ultramafic rocks were subjected to hydrothermal metasomatism, which gave rise to talc-carbonate rocks that appear in the field as veins or irregular patches with characteristic cavernous structure (Fig. 2e).

The ophiolitic metagabbros crop out in a roughly oval-shaped, moderately elevated, allochthonous mass (about 6.5 km long and 2 km wide) in the western part of Wadi El-Mireiwa. In most places, the metagabbro exposures form klippen bounded by footwall exposures of arc metavolcanics, but in some places the metagabbros are observed to

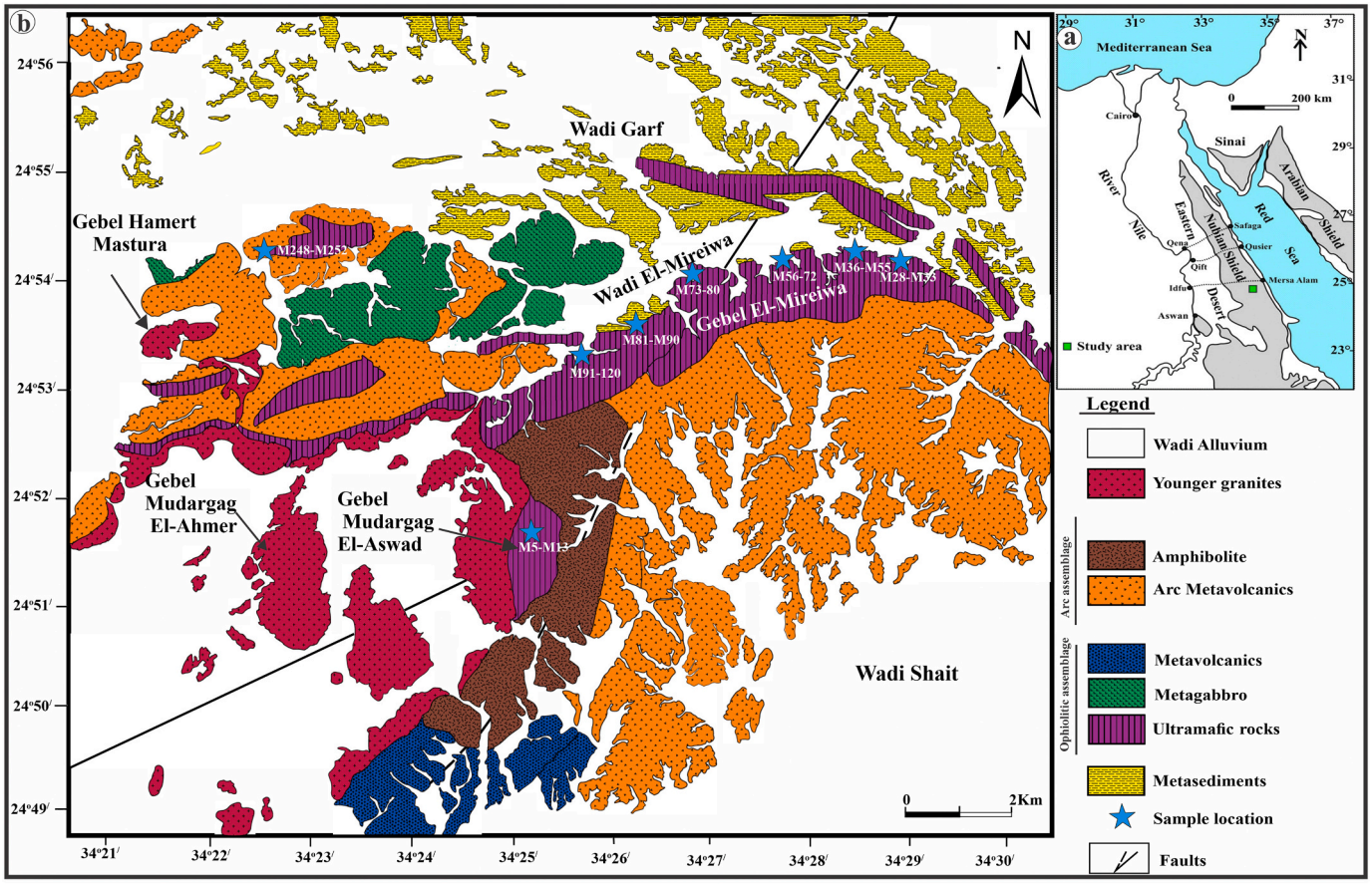

Fig. 1. (a) The outcrop area of the Arabian-Nubian Shield, displaying the study area as a green rectangle. (b) Geologic map of the Wadi El-Mireiwa area (modified after El-Gharbawi, 1988), illustrating the map-scale rock units identified in this work. (For interpretation of the references to color in this figure legend, the reader is referred to the web version of this article.)

overlie the ultramafic rocks and to include pockets of peridotite (Fig. 2f). The gabbros are massive and medium- to coarse-grained. The ophiolitic metavolcanics are present as massive to slightly foliated masses in the southern part of the study area. They are dark grey to dark grayish green, fine- to very fine-grained, and amygdaloidal.

The island arc assemblage comprises metavolcanics and amphibolites. The arc metavolcanics dominate the western and southeastern parts of the mapped area. An elongate outcrop, trending *E*-W and covering about 15 km^2 of the western map area, is bounded to the south by a sharp structural contact with the serpentinized ultramafic rocks. Small mappable masses and sheets of ultramafic rocks are recorded within the western metavolcanic mass (Fig. 1b), defining regions of ophiolitic mélange close to the thrust contact at the base of the ophiolite. To the north, the metavolcanic rocks grade into the metasediments of Wadi Garf; to the east, they are covered by masses of ophiolitic metagabbros; and to the west, they are truncated by the sharp intrusive contact of the Gebel Hamert Mastura syenogranite pluton. The metavolcanic rocks are massive, fine-grained, slightly foliated, and dark grey to dark greenish-grey in color. The southeastern mass of arc metavolcanics covers an area of ~40 km^2, forms low to moderately elevated outcrops, and is dissected by several tributary wadis. The rocks are principally foliated basaltic andesite and metabasalt with minor amounts of metadacite. The arc amphibolite forms a N-S band across the southern central part of the map area. These rocks are medium- to coarse-grained, dark green, and highly sheared where intruded by pink biotite granite.

There are two younger granite plutons in the study area: (l) the Mudargag El-Ahmer pink biotite granite in the southwestern quadrant of the study area intrudes the ultramafic rocks and amphibolite of Gebel Mudargag El-Aswad, whereas (2) the Hamert Mastura yellow muscovite granite in the far western part of the mapped area intrudes the arc metavolcanics.

3. Petrography

A set of 90 thin sections and polished thin sections were prepared for petrographic study of ultramafic rocks selected from the Wadi El-Mireiwa area. Based on the mineralogical composition, the collected ultramafic rocks include variably serpentinized peridotite, serpentinite and clinopyroxenite. As the present study is concerned with the ophiolitic peridotite of the ophiolite, petrographic descriptions are only given here for the serpentinized peridotite and serpentinite samples.

3.1. Peridotites

The peridotites of Wadi El-Mireiwa are all classified as harzburgite and are all extensively serpentinized. They are composed mainly of serpentine minerals with relics of olivine, pyroxene and chromian spinel (Cr-spinel). Tremolite-actinolite and secondary carbonates are locally present. Although no crystals of orthopyroxene were recorded in the examined peridotite sections, the presence of bastite texture in the serpentine indicates alteration after orthopyroxene and supports the inference of harzburgite protoliths (Fig. 3a). Serpentine, mainly antigorite with minor lizardite (verified by Raman spectroscopy, see section 5 below), is massive and occurs as fibrolamellar or scaly fine aggregates preserving relics of olivine and clinopyroxene. Olivine relics occur as rounded to subrounded fine crystals embedded in a matrix of serpentine minerals (Fig. 3b). This olivine prominently displays banded zoning in

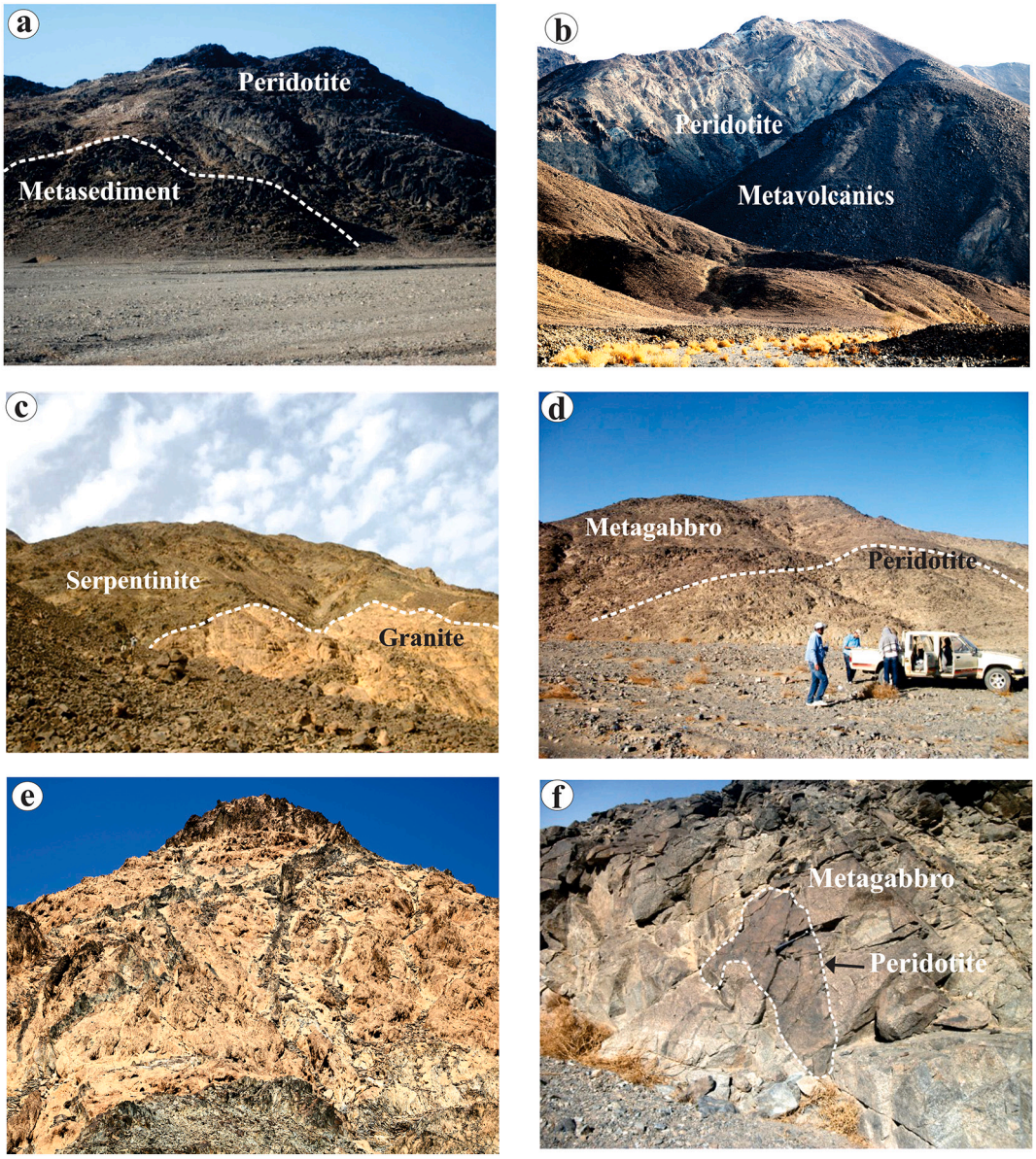

Fig. 2. Field photos showing: (a) structural contact between the ultramafic rocks of Gebel El Mireiwa and the underlying metasediments, (b) the contact between the arc metavolcanics and ultramafic rocks, (c) sharp contact between the younger granite and the serpentinites of Gebel Mudargag El-Aswad, (d) ultramafic rocks overlain by ophiolitic metagabbro, (e) cavernous weathering characteristic to talc carbonates, and (f) pockets of ultramafic rocks within ophiolitic metagabbro.

cross-polarized light (Fig. 3c). Olivine grains are dissected by serpentine veinlets and locally contain opaque inclusions of Cr-spinel. Pyroxene is mainly diopside (Fig. 3d), altered to tremolite-actinolite and chlorite along the rims. Carbonates are mainly calcite with minor magnesite, occurring as sparse crystals, patches and veinlets cutting through serpentine matrix. Opaque minerals are Cr-spinel and magnetite. In reflected light, Cr-spinel occurs as small subhedral to euhedral crystals (Fig. 3e) with grayish white color and reddish-brown internal reflections. Zonation is clearly observed in both reflected light and backscattered electron images (BSE). Zoning, more pronounced in coarse Cr-spinel grains than in finer ones, is indicated by dark cores and bright rims (higher optical reflectivity). The outer rims have sharp contacts with the dark cores of the zoned Cr-spinel grains. EPMA analysis (discussed below) shows that the rims consist of an inner rim of ferritchromite and an outer rim of Cr-magnetite, both alteration products after Cr-spinel. Some Cr-spinel grains contain silicate inclusions, altered to serpentine despite being apparently fully enclosed in spinel (Fig. 3f). Magnetite occurs as disseminated crystals associated with serpentinization of olivine and pyroxene minerals and as outer rims encrusting Cr-spinel grains (Fig. 3e). At the contact with pink biotite granite, metasomatism of the Gebel Mudargag El-Aswad peridotite is indicated by the presence of abundant small globules of green spinel (pleonaste) (Fig. 3g). Pleonaste grains commonly cluster into millimeter-sized aggregates with skeletal or vermicular shapes. Olivine in the metasomatized peridotite forms rounded, equigranular, generally small crystals; they are occasionally aligned to produce a spinifex-like texture. The metasomatic olivine is homogeneous and has textural characteristics comparable to those found in other thermally metamorphosed ultramafic rocks (irregular anhedral habits, elongated crystals, lack of chemical zoning, poikiloblastic and intergrown associations) (e.g., Arai, 1975; Trommsdorff and Evans, 1972).

3.2. *Serpentinites*

Serpentinite samples are completely serpentinized peridotites, lacking any relics of primary silicates. They are fine-grained and massive,

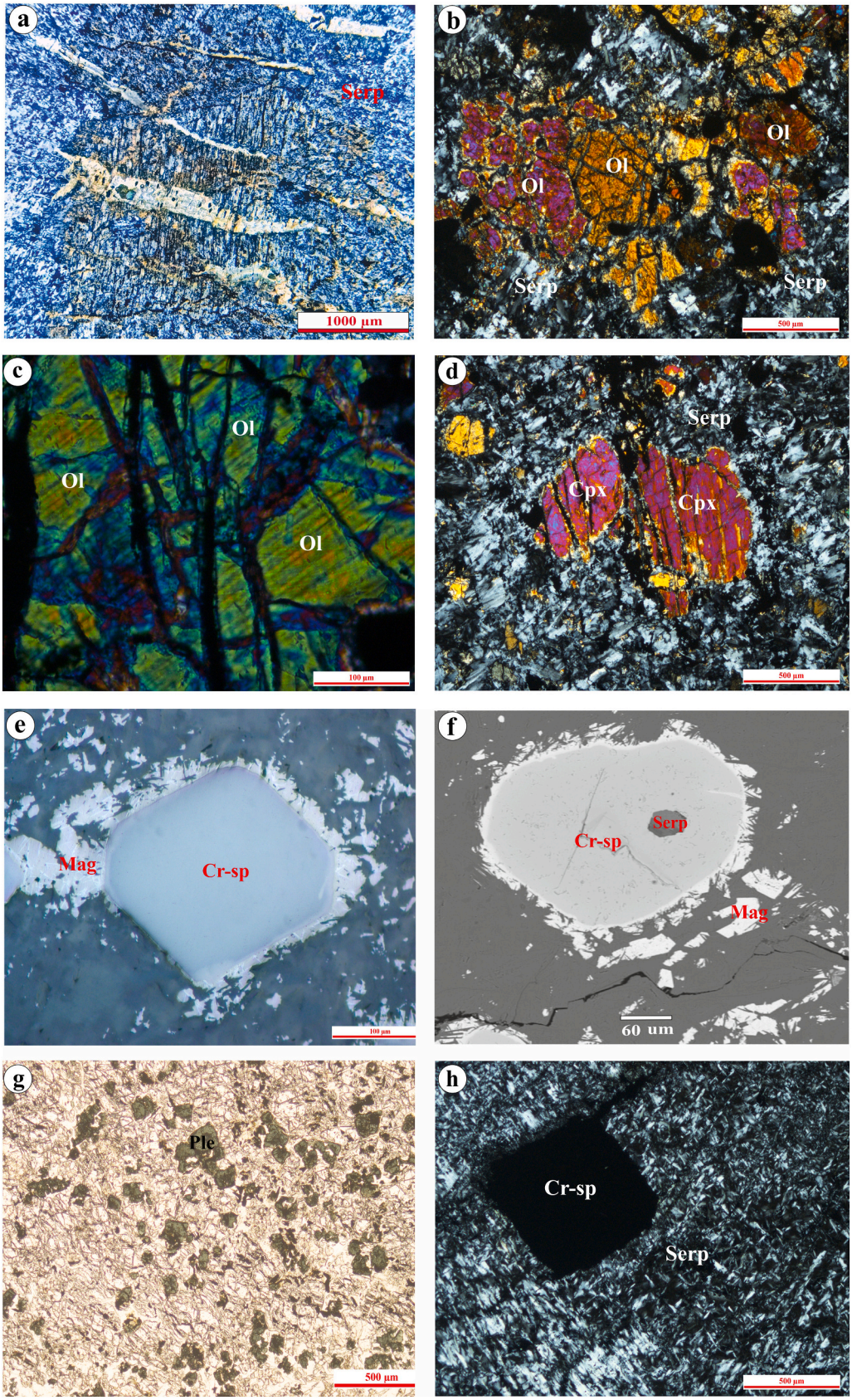

Fig. 3. Photomicrographs for the ultramafic rocks of Wadi El-Mireiwa area (photos (a), (b), (c), (d) and (h) are in cross-polarized light; photo (e) is in reflected light; photo (f) is back-scattered electron image; photo (g) is in plane polarized light): (a) bastite texture after orthopyroxene; (b) relict olivine crystals embedded in a matrix of serpentine minerals; (c) olivine displaying banded zoning; (d) clinopyroxene relics within the serpentinized peridotites; (e) small isotropic euhedral crystals of chromite showing Cr-magnetite rims; (f) inclusions of serpentine minerals from the groundmass within chromite grains; (g) small globular green spinel (pleonaste) within recrystallized olivine; (h) fibro-lamellar aggregates of serpentine (antigorite) in serpentinite. Abbreviations: Ol: olivine, Cpx: clinopyroxene, Serp: serpentine, Cr-sp: chromian spinel, Mag: magnetite, Ple: pleonaste. (For interpretation of the references to color in this figure legend, the reader is referred to the web version of this article.)

consisting mainly of serpentine minerals with variable amounts of carbonates, talc, chlorite and opaques. Antigorite is the essential serpentine mineral (verified by Raman analysis, see section 5). It occurs as scaly or fibrolamellar aggregates (Fig. 3h) and commonly preserves bastite and mesh textures indicating a harzburgite protolith. Carbonates occur as scattered patches and network veinlets (up to 1 mm across) of calcite and magnesite. Talc typically occurs as colorless to very light brown anhedral patches and aggregates with noticeable birefringence and high-order interference colors. Chlorite appears as slightly foliated aggregates of fine elongated flakes, usually colorless to pale green and moderately pleochroic. Opaque minerals are Cr-spinel (Fig. 3h), magnetite and sulfides. Cr-spinel is the most common opaque mineral and shows similar petrographic features to that in serpentinized peridotite samples despite differences in chemistry (see section 6.3). Magnetite is secondary and occurs as streaks or small grains within serpentine, suggesting formation during serpentinization of olivine and pyroxene. Sulfides are the least abundant opaque minerals and are dominantly pentlandite, commonly altered to garnierite and Ni-magnetite.

4. Analytical techniques

Based on the petrographic studies, a set of serpentinized peridotite and serpentinite samples were chosen for analysis of mineral chemistry, serpentine phase identification by Raman spectroscopy, and major and trace element whole-rock geochemistry.

4.1. Electron probe micro analyzer (EPMA)

Eight polished and carbon-coated thin sections (three serpentinized peridotites and five serpentinites) were studied by electron microbeam techniques. We used a combination of Scanning Electron microscopy (SEM) — for back-scattered electron (BSE) imaging and Energy Dispersive X-ray Spectroscopy (EDS) — and electron probe microanalyses (EPMA). Both instruments are hosted by the Division Analytical Facility of the Division of Geological and Planetary Sciences, California Institute of Technology (Caltech), USA. The SEM is a Zeiss 1550VP instrument with an Oxford X-Max Si-drift detector. The EPMA is a JEOL JXA-8200 equipped with five wavelength dispersive spectrometers (WDS). It was operated with accelerating voltage of 15 kV with a 25 nA focused (~1 μm) beam, with a counting time of 20 s on-peak for each analyzed element. Analyzed phases include the relict primary minerals (olivine, pyroxene and Cr-spinel) and secondary minerals (serpentine). Accepted natural and synthetic mineral standards were used for calibration, including synthetic forsterite, fayalite, Mn-olivine, anorthite, TiO_2, and Cr_2O_3 as well as natural Amelia albite and Asbestos microcline. Quartz, Al_2O_3 and MgO provided additional control points for the mean atomic number (MAN) background subtraction method. The CITZAF matrix correction routine was applied.

4.2. Raman spectroscopy

The serpentine phases of the serpentinized ultramafic rocks of Wadi El-Mireiwa were differentiated using Raman spectroscopy (Renishaw InVia micro-Raman spectrometer with 514 nm Ar-ion laser) at the GPS Division, Caltech, USA. Phase identifications were verified using the reference spectra of Petriglieri et al. (2015) in both the 200–1100 cm^{-1} silicate vibration range and the 3550–3850 cm^{-1} OH-stretching region.

4.3. XRF and ICP-MS

Based on the petrographic studies, eight ultramafic rock samples were selected for major, trace and rare earth elements analyses at Caltech. Major and minor oxides were determined using a Panalytical Zetium Wavelength-dispersive XRF spectrometer on fused glass beads. Samples were crushed in a tungsten carbide jaw crusher and milled to powder in a Retsch planetary ball mill in agate mortars. Loss on Ignition (LOI) was determined by weight loss after 1 h at 1050 °C. Samples were mixed with 9 times their weight in 66.67% $Li_2B_4O_7$–32.83% $LiBO_2$–0.50% LiI flux and fused at 1200 °C. The XRF protocol was calibrated against 21 USGS rock standards. USGS standards BCR-2, AGV-2 and GSP-2 were routinely analyzed along with unknowns for quality control and drift correction. Major elements are reproducible with this method to better than 0.5% and are considered accurate to 1%.

After XRF measurements, 25 ± 1 mg chips of the fused glass XRF beads were placed in new polypropylene tubes and dissolved in 2 mL of 3:1 hydrofluoric and nitric acid solution. Samples were dried by heating at 95 °C for five hours. They were then resuspended in 10 mL dilute 5% nitric and 0.1% hydrofluoric acid and heated at 50 °C for 1 h to aid in dissolution. and then brought to a final volume of 30 mL. Trace and Rare earth elements (REE) concentrations were obtained using an Agilent Technologies 8800 triple quadrupole ICP-MS. A calibration curve for each element was created using four USGS standards, each containing a known concentration of the element. To control for quality, additional USGS Reference materials AGV-2, BCR-2, GSP-1, and RGM-2 were also run and treated as a secondary quality control. Most trace elements and REE with this protocol have detection limits ~0.1 μg g^{-1}, reproducibility of 2%, and external accuracy of 5% RSD.

5. Serpentine mineralogy

The ultramafic rocks of Wadi El-Mireiwa area are all partly to completely serpentinized. The serpentine species in our samples were specifically identified by Raman spectroscopy. For the discrimination of antigorite from other serpentine polymorphs, the presence of a peak at ~1044 cm^{-1} in the low wavenumber region has proven to be decisive (Petriglieri et al., 2015). The Raman spectra, especially the presence of a peak at 1041 cm^{-1} in the low wavenumber region and peaks at 3661–3665 cm^{-1} accompanied by smaller peaks at 3693–3695 cm^{-1} in the high wavenumber region (Fig. 4), indicate that both serpentinized harzburgite and serpentinite samples are dominated by antigorite. However, in the low wavenumber region, the Raman spectra of antigorite in serpentinite (Fig. 4e-h) display more sharp peaks than those of the antigorite in serpentinized peridotite (Fig. 4a-d), indicating a higher degree of crystalline order.

6. Mineral chemistry

6.1. Olivine

According to Arai (1975), when olivine is a primary phase in residual mantle peridotites it appears homogenous in appearance, with Fo, NiO, and MnO concentrations close to 90–92, 0.4 wt%, and 0.1 wt%, respectively. However, the analyzed olivine from the peridotites in the Wadi El-Mireiwa area shows heterogeneous chemistry, with marked intracrystalline variation in forsterite (Fo), NiO, and MnO contents (Fig. 5a & b and representative analyses in Table 1; complete data set is given in Supplementary Table S1). These marked changes in major and minor element abundance are developed along specific crystallographic orientations in the olivine grains, resulting in prominently banded zoning patterns (Figs. 3c and 6a). Narrow Mg-enriched stripes, appearing dark in BSE images, alternate with broader zones that constitute the bulk of the olivine grains, have lower MgO content, and appear bright in BSE images (Fig. 6a & b). The Mg-enriched stripes have higher Fo (93–99, average 95.5) and MnO contents (0.24–1.31 wt%, average 0.52 wt%) compared with the bulk olivine zones (Fo = ~86 to 92, average = 89; MnO = 0.19 to 0.44 wt%, average 0.30 wt%). The Mg-enriched stripes have highly variable NiO contents (0.02 to 0.28 wt%) extending to extreme depletion but not apparently correlated with Fo or MnO. The bulk olivine zones, by contrast, have a narrow range of NiO contents (0.22 to 0.32 wt%, average 0.25 wt%) that also do not correlate with Fo or MnO. Given the finely intergrown texture of the normal olivine and

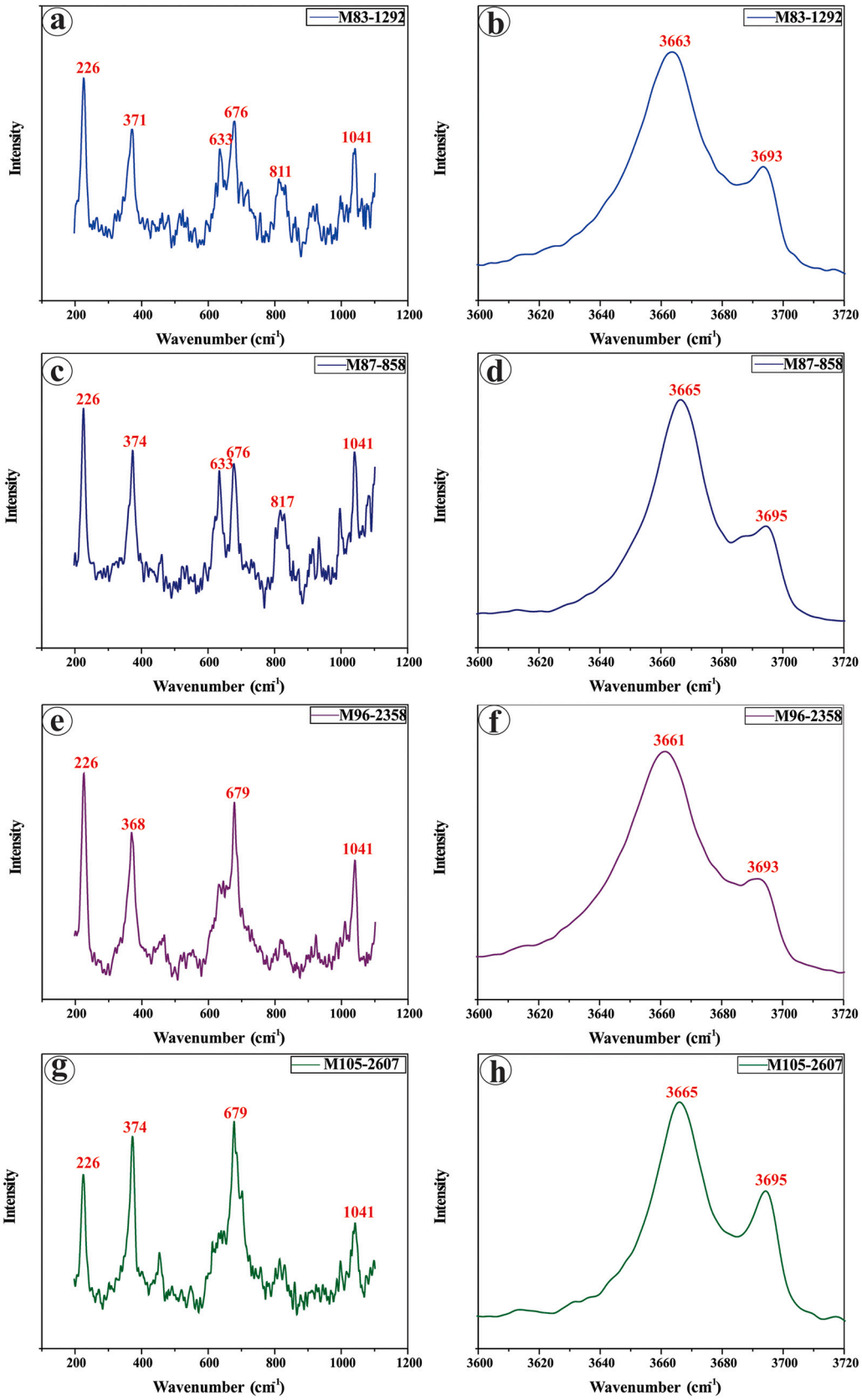

Fig. 4. Raman spectra of serpentine minerals (antigorite) in Wadi El-Mireiwa (a-d) serpentinized peridotites and (e-h) serpentinites.

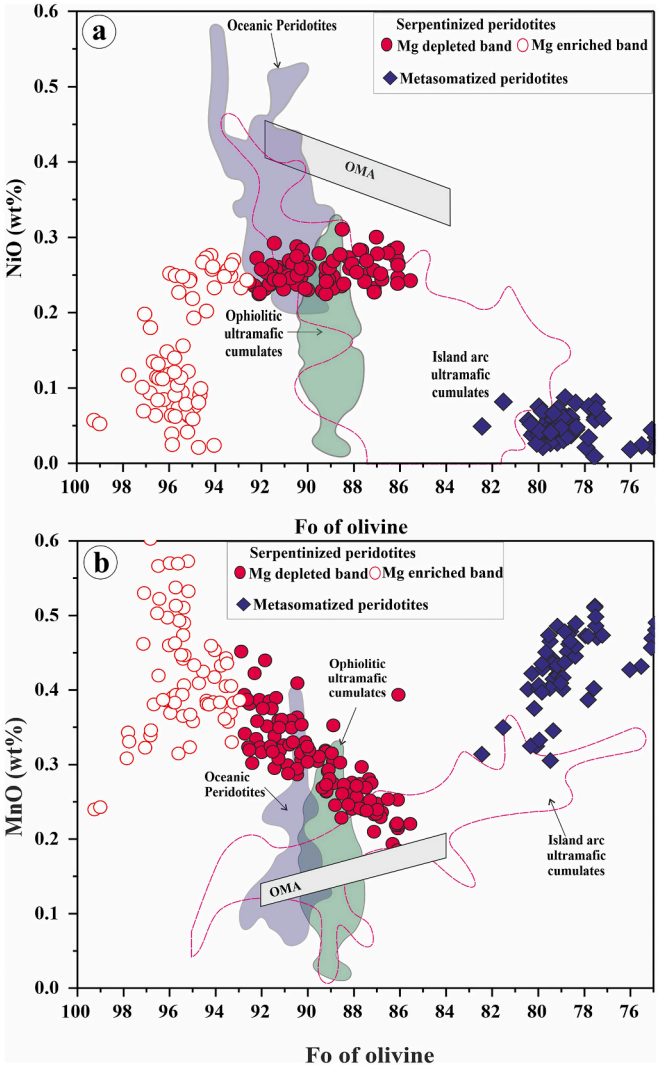

Fig. 5. (a) NiO (wt%) vs. Fo content. The olivine mantle array (OMA) is after Takahashi et al. (1987); Fields of oceanic peridotite, ophiolitic ultramafic cumulate and island arc ultramafic cumulate are after Maurice et al. (2021). (b) MnO (wt%) vs. Fo content. The olivine mantle array (OMA) is after Takahashi et al. (1987); fields of oceanic peridotite, ophiolitic ultramafic cumulate and island arc ultramafic cumulate are after Maurice et al. (2021).

the Mg-enriched bands, it is likely that some of the measured points represent mixed analytical volumes. The NiO content of the bulk olivine is systematically lower than that of typical mantle olivine (Takahashi et al., 1987) but comparable to the cumulate harzburgites of the Um Salem ophiolite in the Central Eastern Desert (Ali et al., 2020).

The metasomatized peridotite samples near the contact with the granite intrusion contain an entirely distinct population of olivine with plainly different chemical compositions and petrographic features. It is ferroan olivine with Fo content from 73 to 82 (Table S1). Its NiO and MnO contents vary from 0.09 to 0.01 wt%, and from 0.31 to 0.55 wt%, respectively, and do not plot on the extension of the trends through the olivine compositions of the unmetasomatized peridotites (Fig. 5a and b). We attribute this population of olivine compositions to contact metasomatism in proximity to the granite intrusion (e.g., Ahmed et al., 2012).

6.2. Pyroxenes

The only pyroxene observed in the serpentinized peridotite samples is relict clinopyroxene; chemical analyses of these relics are given in Supplementary Table S2. The range of clinopyroxene compositions is limited, restricted to $En_{45-55}Fs_{2-6}Wo_{42-50}$. Each grain is homogeneous, with no resolvable core-rim zoning. According to the conventional classification of Morimoto et al. (1988), this material is mainly diopside (Supplementary Fig. S1). With TiO_2 contents <1 wt%, they resemble clinopyroxene from non-alkaline rocks. Their Cr_2O_3 (0.29–0.92 wt%, average 0.56 wt%) and Al_2O_3 contents (1.1–3.2 wt%, average 2.3 wt%) confirm their primary origin, because metamorphic clinopyroxenes have lower Cr_2O_3 (<0.4 wt%) and Al_2O_3 (<0.5 wt%) contents (Nozaka, 2010). The Mg# (88.2–95.8) of the clinopyroxene analyses is largely similar to those of ophiolitic cumulates (Allahyari et al., 2014; Parlak et al., 1996). There is a negative correlation between Al_2O_3 content and Mg# that resembles the trend documented in wehrlites of the Mersin ophiolite (Parlak et al., 1996) (Fig. 7a).

6.3. Chromian spinels

The chemical compositions and structural formulae of primary chromian spinel and its alteration products in serpentinized peridotite and serpentinite are given in Supplementary Table S3. The Cr^{+3}-Fe^{+3}-Al^{+3} spinel classification diagram (Supplementary Fig. S2) of Stevens (1944) shows that the fresh spinel ranges from Cr-spinel to Al-chromite, whereas the altered spinel plots in the Fe-chromite and Cr-magnetite fields. BSE images and detailed compositional profiles using high resolution X-ray intensity maps (see section 9.4) of Cr-spinel grains in serpentinized peridotite reveal up to four conspicuous zones: a fresh inner core mantled by a metasomatized outer core, followed by a ferritchromite mantle and a Cr-magnetite outer rim. These Cr-spinel grains display reverse zoning from the fresh inner core to the metasomatized outer core, marked by an increase in MgO (on average, 10.4 to 13.5 wt%), a decrease in FeO* (31.6 to 27.7 wt%), and a slight decrease in Al_2O_3 (21.2 to 20.1 wt%). Cr_2O_3 (32.2 wt% vs. 32.4 wt%) and TiO_2 (~0.3 wt %) contents do not show any significant variation within the core region. On average, the fresh inner cores of Cr-spinel grains in serpentinized peridotite have lower Mg# (0.51) and Cr# (0.45) than the metasomatized outer cores (Mg# = 0.67; Cr# = 0.53). This variation in composition from inner to outer core of Cr-spinel grains is attributed to fluid-rock interaction (metasomatism) in the supra-subduction zone setting (Gamal El Dien et al., 2019). In the ferritchromite zones and highly altered Cr-magnetite rims, the compositional change is manifested by strong decreases in Al_2O_3, MgO, and Cr_2O_3 contents compensated by increases in FeO and Fe_2O_3. This alteration is attributed to element mobility during greenschist facies metamorphism.

In contrast with those in serpentinized peridotite, the cores of Cr-spinel grains in fully serpentinized samples display normal zoning in which Mg and Al decrease whereas Fe and Cr# increase from core to rim. However, as in serpentinized peridotite, the fresh Cr-spinel cores in serpentinite are surrounded by variably developed thin ferritchromite zones, followed by Cr-magnetite rims. Compared with those in serpentinized peridotite, the fresh Cr-spinel cores in serpentinite samples have higher Cr_2O_3 contents (39.5–45.3 wt%, average 43.1 wt%), lower Al_2O_3 (11.5–21.5 wt%, average 15.5 wt%) and MgO (4.4–10.2 wt%, average 7.1 wt%) contents, and lower Mg# (0.24–0.50, average = 0.36). FeO* contents (27.6–35.9 wt%, average = 31.4 wt%) and TiO_2 contents (average = 0.24 wt%) are similar in Cr-spinel cores in the two sample categories. Although the full range of Cr# measurements of these fresh cores (0.55–0.72) partly overlaps those from serpentinized peridotite (0.17–0.63), the average (Cr# = 0.65) in serpentinite samples is markedly higher than that in serpentinized peridotite samples (Cr# = 0.45). There is one exception to these Cr-spinel compositions in serpentinite: sample M248, which was collected from the northwestern part of the study area, has markedly lower TiO_2 content (0.00–0.04 wt%, average 0.01 wt%), reflecting a strongly depleted character. The chemical trends in the altered rims of Cr-spinel grains in serpentinite are similar to those in serpentinized peridotite.

Table 1
Representative elecron microprobe data of the olivine from the Wadi El-Mireiwa peridotites, South Eastern Desert, Egypt.

Rock Type	Serpentinized Peridotites															
Sample No	M84								M87							
	Ol(bulk)	Ol(zone)	Ol(bulk)	Ol(zone)	Ol(bulk)	Ol(zone)	Ol(bulk)	Ol(zone)	Ol(Bulk)	Ol(zone)	Ol(bulk)	Ol(zone)	Ol(bulk)	Ol(zone)	Ol(bulk)	Ol(zone)
Grain No	Grain No 1				Grain No 2				Grain No 1				Grain No 2			
spot	126	85	119	82	142	159	163	190	831	834	838	844	969	986	967	987
SiO_2	42.28	42.31	41.72	42.77	41.25	42.99	41.32	42.61	40.46	41.84	40.96	40.96	39.99	41.07	40.63	41.28
TiO_2	0.00	0.00	0.01	0.01	0.01	0.01	0.00	0.01	0.00	0.00	0.01	0.02	0.00	0.01	0.00	0.00
Al_2O_3	0.02	0.07	0.01	0.08	0.01	0.03	0.00	0.02	0.00	0.00	0.00	0.00	0.01	0.11	0.00	0.00
Cr_2O_3	0.00	0.02	0.00	0.00	0.00	0.02	0.00	0.00	0.00	0.00	0.00	0.00	0.00	0.00	0.00	0.00
FeO	8.75	3.11	8.04	4.02	10.14	2.82	9.71	3.45	10.74	4.05	9.53	6.72	12.11	4.11	9.00	5.29
MnO	0.33	0.60	0.32	0.63	0.27	0.52	0.30	0.50	0.30	0.37	0.33	0.38	0.25	0.39	0.36	0.41
MgO	48.50	53.39	49.34	52.74	47.77	54.17	49.09	54.05	48.26	54.07	48.72	51.78	47.73	53.49	49.45	53.33
NiO_2	0.27	0.09	0.24	0.06	0.23	0.10	0.23	0.11	0.23	0.25	0.23	0.27	0.24	0.02	0.25	0.02
CaO	0.00	0.00	0.01	0.01	0.01	0.00	0.00	0.01	0.04	0.02	0.02	0.04	0.03	0.01	0.05	0.00
Na_2O	0.00	0.00	0.00	0.00	0.00	0.01	0.01	0.00	0.00	0.01	0.01	0.01	0.00	0.00	0.01	0.00
K_2O	0.00	0.00	0.24	0.06	0.23	0.10	0.23	0.11	0.00	0.00	0.01	0.00	0.00	0.16	0.00	0.20
Total	100.19	99.66	99.74	100.33	99.72	100.68	100.68	100.77	100.05	100.62	99.82	100.18	100.36	99.38	99.75	100.52
No of cations on the basis of four oxygen atoms																
Si	1.03	1.01	1.02	1.02	1.01	1.01	1.01	1.01	1.00	1.00	1.01	0.99	0.99	0.99	1.00	0.99
Ti	0.00	0.00	0.00	0.00	0.00	0.00	0.00	0.00	0.00	0.00	0.00	0.00	0.00	0.00	0.00	0.00
Al	0.00	0.00	0.00	0.00	0.00	0.00	0.00	0.00	0.00	0.00	0.00	0.00	0.00	0.00	0.00	0.00
Cr	0.00	0.00	0.00	0.00	0.00	0.00	0.00	0.00	0.00	0.00	0.00	0.00	0.00	0.00	0.00	0.00
Fe	0.18	0.06	0.16	0.08	0.21	0.06	0.20	0.07	0.22	0.08	0.20	0.14	0.25	0.08	0.18	0.11
Mn	0.01	0.01	0.01	0.01	0.01	0.01	0.01	0.01	0.01	0.01	0.01	0.01	0.01	0.01	0.01	0.01
Mg	1.76	1.90	1.79	1.87	1.75	1.90	1.78	1.90	1.77	1.92	1.78	1.87	1.76	1.92	1.81	1.90
Ca	0.00	0.00	0.00	0.00	0.00	0.00	0.00	0.00	0.00	0.00	0.00	0.00	0.00	0.00	0.00	0.00
Na	0.00	0.00	0.00	0.00	0.00	0.00	0.00	0.00	0.00	0.00	0.00	0.00	0.00	0.00	0.00	0.00
K	0.00	0.00	0.00	0.00	0.00	0.00	0.00	0.00	0.00	0.00	0.00	0.00	0.00	0.00	0.00	0.00
Ni	0.00	0.00	0.00	0.00	0.00	0.00	0.00	0.00	0.00	0.00	0.00	0.00	0.00	0.00	0.00	0.00
Total	2.97	2.99	2.98	2.98	2.99	2.99	2.99	2.99	3.00	3.00	2.99	3.01	3.01	3.01	3.00	3.01
Fo%	90.80	96.83	91.62	95.90	89.36	97.16	90.01	96.54	88.90	95.96	90.11	93.21	87.53	95.86	90.73	94.73
Mg#	0.91	0.97	0.92	0.96	0.89	0.97	0.90	0.97	0.89	0.96	0.90	0.93	0.88	0.96	0.91	0.95

Rock Type	Serpentinized peridotite												Metasomatized	
Sample No	M88												M13	M8
	Ol(bulk)	Ol(zone)	Ol(bulk)	Ol(zone)	Ol(bulk)	Ol(zone)	Ol(bulk)	Ol(zone)	Ol(bulk)	Ol(zone)	Ol(bulk)	Ol(zone)	ol(bulk)	ol(bulk)
Grain No	Grain No 1				Grain No 2				Grain No 3					
spot	514	526	515	520	687	565	690	571	135	90	148	155	791	684
SiO_2	41.37	43.02	41.48	42.99	40.65	43.31	41.51	42.35	40.66	41.88	41.69	42.90	41.03	38.79
TiO_2	0.01	0.00	0.01	0.00	0.00	0.00	0.00	0.00	0.00	0.08	0.04	0.01	0.00	0.00
Al_2O_3	0.01	0.01	0.00	0.00	0.00	0.29	0.00	0.00	0.00	1.02	0.00	0.00	0.01	0.01
Cr_2O_3	0.01	0.03	0.04	0.01	0.00	0.02	0.03	0.00	0.00	0.27	0.00	0.00	0.01	0.00
FeO	12.92	3.16	10.57	5.55	13.22	2.23	9.25	3.72	13.11	0.97	9.42	2.93	17.88	22.61
MnO	0.19	0.35	0.28	0.39	0.22	0.33	0.41	0.39	0.22	0.24	0.31	0.32	0.38	0.47
MgO	45.75	53.83	48.33	52.45	46.23	54.55	49.25	54.13	45.68	54.48	49.17	54.30	40.59	38.22
NiO_2	0.28	0.18	0.26	0.27	0.27	0.12	0.25	0.11	0.29	0.05	0.26	0.20	0.04	0.02
CaO	0.02	0.02	0.01	0.02	0.00	0.03	0.02	0.01	0.03	0.05	0.02	0.03	0.05	0.00
Na_2O	0.00	0.00	0.00	0.00	0.00	0.00	0.00	0.00	0.00	0.02	0.00	0.01	0.02	0.00

(*continued on next page*)

Table 1 (*continued*)

Rock Type	Serpentinized peridotite												Metasomatized	
Sample No	M88												M13	M8
	Ol(bulk)	Ol(zone)	Ol(bulk)	Ol(zone)	Ol(bulk)	Ol(zone)	Ol(bulk)	Ol(zone)	Ol(bulk)	Ol(zone)	Ol(bulk)	Ol(zone)	ol(bulk)	ol(bulk)
Grain No	Grain No 1				Grain No 2				Grain No 3					
K_2O	0.00	0.00	0.00	0.00	0.00	0.00	0.00	0.00	0.00	0.01	0.00	0.00	0.01	0.00
Total	100.57	100.60	100.97	101.68	100.59	100.89	100.73	100.71	99.99	99.08	100.92	100.70	100.02	100.13
No of cations on the basis of four oxygen atoms														
Si	1.02	1.02	1.01	1.02	1.01	1.02	1.01	1.00	1.01	1.00	1.01	1.01	1.04	1.01
Ti	0.00	0.00	0.00	0.00	0.00	0.00	0.00	0.00	0.00	0.00	0.00	0.00	0.00	0.00
Al	0.00	0.00	0.00	0.00	0.00	0.01	0.00	0.00	0.00	0.03	0.00	0.00	0.00	0.00
Cr	0.00	0.00	0.00	0.00	0.00	0.00	0.00	0.00	0.00	0.01	0.00	0.00	0.00	0.00
Fe	0.27	0.06	0.22	0.11	0.27	0.04	0.19	0.07	0.27	0.02	0.19	0.06	0.38	0.49
Mn	0.00	0.01	0.01	0.01	0.00	0.01	0.01	0.01	0.00	0.00	0.01	0.01	0.01	0.01
Mg	1.68	1.89	1.75	1.85	1.70	1.90	1.78	1.91	1.69	1.93	1.78	1.91	1.53	1.48
Ca	0.00	0.00	0.00	0.00	0.00	0.00	0.00	0.00	0.00	0.00	0.00	0.00	0.00	0.00
Na	0.00	0.00	0.00	0.00	0.00	0.00	0.00	0.00	0.00	0.00	0.00	0.00	0.00	0.00
K	0.00	0.00	0.00	0.00	0.00	0.00	0.00	0.00	0.00	0.00	0.00	0.00	0.00	0.00
Ni	0.00	0.00	0.00	0.00	0.00	0.00	0.00	0.00	0.00	0.00	0.00	0.00	0.00	0.00
Total	2.98	2.98	2.99	2.98	2.99	2.98	2.99	3.00	2.99	2.99	2.99	2.99	2.96	2.99
Fo%	86.32	96.81	89.07	94.40	86.17	97.75	90.46	96.29	86.13	99.01	90.29	97.06	80.17	75.07
Mg#	0.86	0.97	0.89	0.94	0.86	0.98	0.90	0.96	0.86	0.99	0.90	0.97	0.80	0.75

6.4. Serpentine

The chemical compositions of serpentine minerals from the ultramafic rocks of Wadi El-Mireiwa are given in supplementary Table S4. Al_2O_3 contents of serpentine are low: on average, 0.97 wt% in serpentinized peridotite and 0.62 wt% in serpentinite. SiO_2 contents (average 42.5 wt% in serpentinized peridotite, average 42.3 wt% in serpentinite) and MgO contents (average 39.7 wt% in serpentinized peridotite, 38.5 wt% in serpentinite) do not differ significantly between rock types. On the other hand, serpentine in serpentinized peridotite displays significantly lower FeO* (0.43–4.6 wt%, average 1.3 wt%) than in serpentinite (0.76–8.5 wt%, average 3.4 wt%).

7. Geochemistry

The whole-rock geochemistry of a representative group of eight ultramafic rocks from the study area is given in Supplementary Table S5. The ultramafic rocks are mainly harzburgite based on their normative whole rock chemistry (Fig. 8). Although three samples (M84, M108, M252) plot in the lherzolite field, this is attributed to CaO in secondary carbonates. The variably high LOI values (9.5–17.0 wt%, average 13.5 wt%) extend from values less than that of stoichiometric serpentine (~13 wt% structural H_2O), reflecting preservation of significant primary phases in some samples, to values greater than that of pure serpentine, reflecting the additional influence of carbonate. The chemical compositions of the serpentinized peridotite samples span a remarkable range in SiO_2 contents, from 33.6 to 40.6 wt% (average 36.8 wt%). MgO contents are high (34.0 to 38.2 wt%, average 36.6 wt%). Most other oxides are uniformly low: Al_2O_3 (0.42 to 0.85 wt%, average 0.56 wt%), TiO_2 (0.01 to 0.04 wt%, average 0.03 wt%), and CaO (average 1.49 wt %). There are two samples (M87 and M88) with anomalously high Al_2O_3 contents that are attributed to the presence of chlorite, high modal clinopyroxene content, and high-Al Cr-spinel grains in these two samples.

The bulk-rock Mg# of the serpentinized peridotite samples ranges from 0.87 to 0.92. Whole-rock ratios of MgO/SiO_2 (from 0.87 to 1.09) and Al_2O_3/SiO_2 (0.01–0.02) ratios (Fig. 9) are similar to those of modern fore-arc peridotites (Niu, 2004; Parkinson and Pearce, 1998; Pearce et al., 2000), but the large variation in MgO/SiO_2 at nearly constant Al_2O_3/SiO_2 in the serpentinite samples is inconsistent with control of the bulk chemical variation by melt extraction; another process or processes must have modified the compositions. Most of the REE and several trace elements are below the detection limits of the analytical protocol used, which indicates that the formation of these ultramafic rocks involved extensive melt extraction or that they crystallized from (or reacted with) a highly depleted liquid. The metasomatism of samples proximal to the granite intrusion resulted in a marked increase in Al_2O_3 (up to 18.95 wt %) and decreases in MgO (down to 28.30 wt%) and Mg# (0.82) in the metasomatized samples (Table S5).

8. Oxygen fugacity

The fO_2 values of Wadi El-Mireiwa peridotite were estimated using the electron microprobe analysis of coexisting Cr-spinel and olivine in serpentinized peridotites (Ballhaus et al., 1990). For each sample, fO_2 values are estimated twice. First, using unmetasomatized Cr-spinel and the bulk of the fresh olivine crystals, and second using metasomatized outer-core Cr-spinel zones and the Mg-enriched olivine band compositions. That is, assuming the development or reverse zoning and modified outer cores in Cr-spinel and the development of the Mg-enriched bands in olivine record the same metasomatic event, these samples offer the opportunity to evaluate the oxidation state of the rock both before and during interaction with metasomatic fluids. The fO_2 results are given in log units relative to the FMQ (fayalite-magnetite-quartz) buffer at 1.0 GPa pressure, i.e. $\Delta \log fO_2$(FMQ). The calculated $\Delta \log fO_2$(FMQ) values vary from +2.48 to +2.67 for the unmetasomatized Cr-spinel-olivine pairs and from +3.75 to +4.53 for the metasomatized parts of

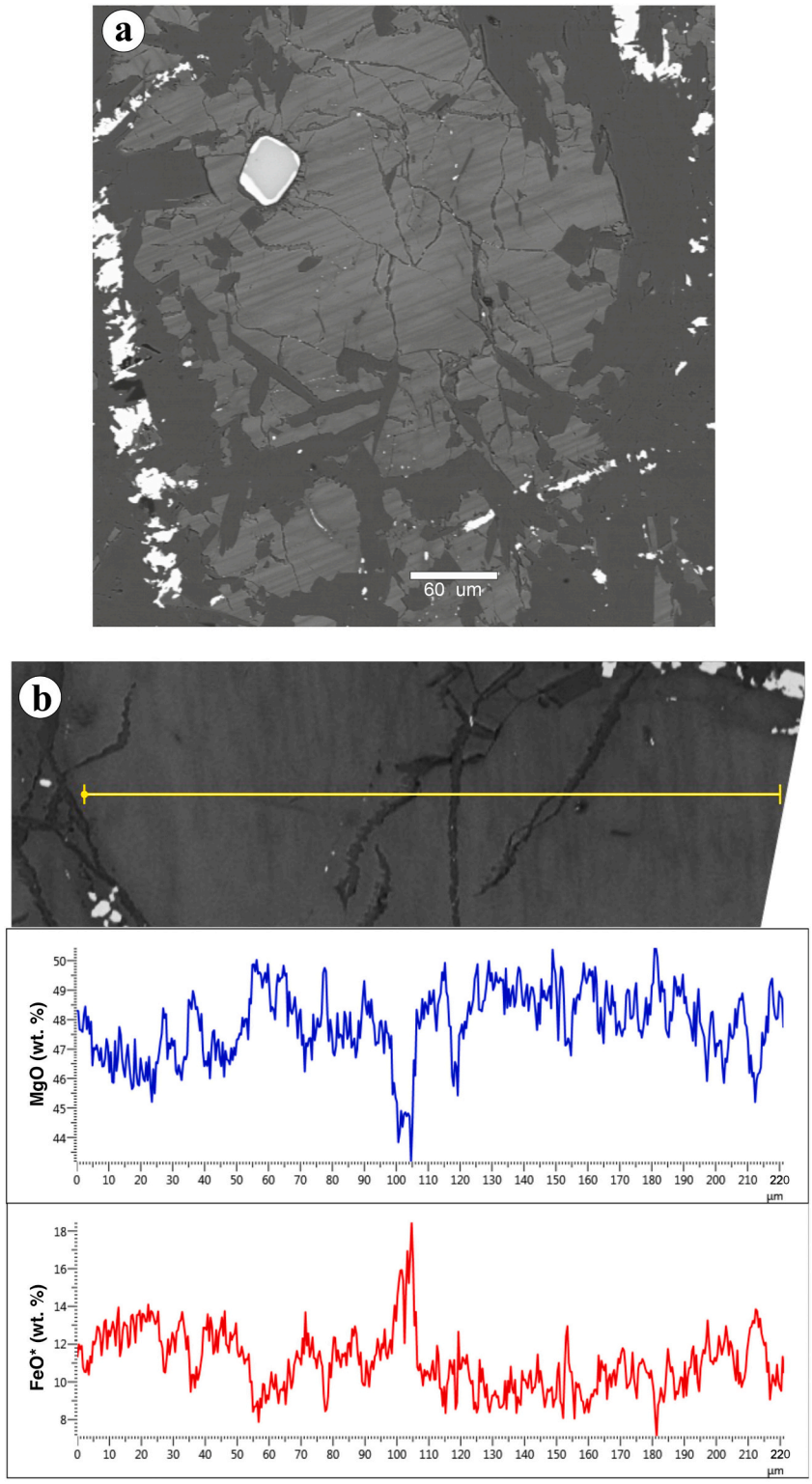

Fig. 6. (a) BSE image of banded olivine with chromite inclusion, dissected by serpentine blades and displaying alternation between Mg-enriched (dark contrast) and normal (lighter contrast) bands; (b) High-resolution, high-precision X-ray line scan for banded olivine showing the distribution of MgO and FeO.

metasomatized Cr-spinel and Mg-rich bands in olivine.

9. Discussion

9.1. Tectonic setting

Because the Egyptian ophiolites represent key lithologies for reconstructing the geodynamic evolution of the pan-African belt of the Arabian Nubian Shield (ANS), several studies have been dedicated to inferring their origin and tectonic setting. The results of these studies, however, have been contradictory. A wide range of tectonic settings has been claimed, including both open-ocean ridges unrelated to subduction (e.g., Zimmer et al., 1995) and supra-subduction zone spreading centers (e.g., Azer and Stern, 2007). The supra-subduction zone setting is,

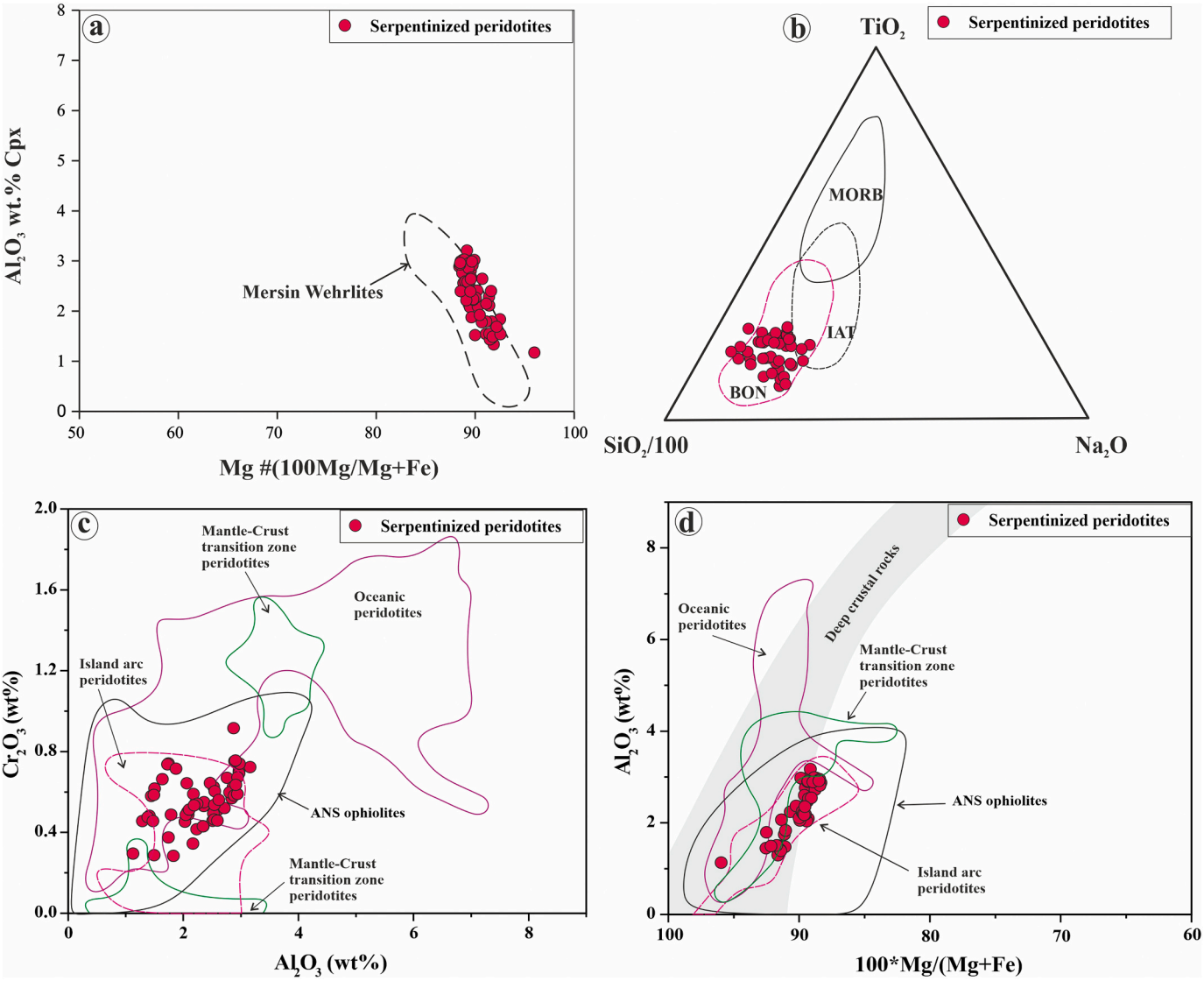

Fig. 7. (a) Mg# vs. Al_2O_3 of clinopyroxene from Wadi El-Mireiwa serpentinized peridotites; the field of the Mersin wehrlite (after, Parlak et al., 1996). (b) TiO_2–Na_2O–SiO_2/100 ternary diagram for clinopyroxene (after Beccaluva et al., 1989). WOPB = within-ocean plate basalts; MORB = mid-ocean ridge basalts; IAT = island arc tholeiites; BON = boninites + basaltic andesites and andesites from intra-oceanic forearcs. (c) Cr_2O_3 vs. Al_2O_3 in clinopyroxene. (d) Al_2O_3 vs. 100*Mg/(Mg + Fe) in clinopyroxene. Deep crustal rocks field (after DeBari and Coleman, 1989) and fields of oceanic peridotite, mantle-crust transition zone peridotite, ANS ophiolites and island arc peridotites are after Maurice et al. (2021).

however, now widely accepted among recent studies on the Neoproterozoic ophiolites of Egypt (e.g., Abdel-Karim et al., 2016; Ahmed et al., 2012; Azer and Stern, 2007). Ongoing debate centers on attempts to distinguish back-arc settings (e.g., Basta et al., 2011) from fore-arc settings (e.g., Abd El-Rahman et al., 2009; Abdel-Karim et al., 2016; Ali et al., 2020; Azer and Stern, 2007; Gahlan et al., 2015).

The mineral chemistry of relict primary minerals (olivine, Cr-spinel and pyroxenes) in altered ultramafic rocks offers a number of useful petrogenetic indicators of tectonic setting (e.g., Saccani and Tassinari, 2015). On discrimination diagrams related to Cr-spinel mineral chemistry, we plot only the fresh cores of Cr-spinel grains, excluding rim regions as well as cores that have been affected by metasomatic fluids. In most diagrams, we find three distinct populations of Cr-spinel in the Wadi El-Mireiwa ultramafic rocks. The serpentinized peridotite samples contain high- and low-Cr_2O_3 groups (samples M87 and M88 define the low-Cr_2O_3 group) with roughly the same TiO_2 contents, whereas the serpentinite samples contain only high-Cr_2O_3 analyses but divide into high- and low-TiO_2 groups. The high-Cr_2O_3, high-TiO_2 groups from the two rock types mostly overlap (Fig. 10a). All the analyses plot within the large and permissive field of oceanic peridotites on a Cr_2O_3 vs. TiO_2 diagram, whereas only the low-Cr_2O_3 group from serpentinized peridotite is consistent with the mafic-ultramafic intrusions of the Eastern Desert and Sinai, and only the high-Cr_2O_3, high-TiO_2 group that occurs in both rock types is consistent with the field of Oman ultramafic cumulates (OUC).

The Al_2O_3 and TiO_2 contents of Cr-spinel have been used to differentiate between peridotites from supra-subduction zone (SSZ) and mid-oceanic ridge (MOR) settings (Kamenetsky et al., 2001). On a TiO_2 vs. Al_2O_3 tectonic discrimination diagram (Fig. 10b), the fresh Cr-spinel of most serpentinites and serpentinized peridotite samples plot within the SSZ peridotite field, but the high-Al_2O_3 content of Cr-spinel in samples M87 and M88 pushes them over towards the MOR peridotite field. The very low TiO_2 contents of several Cr-spinel analyses in the serpentinite samples confirm their highly depleted character, a trait closely associated with SSZ tectonic settings (Fig. 10c).

Given the SSZ character of most of the samples, we turn to the more subtle question of whether they developed in back-arc or fore-arc setting. In a fore-arc environment, ophiolites may be emplaced more

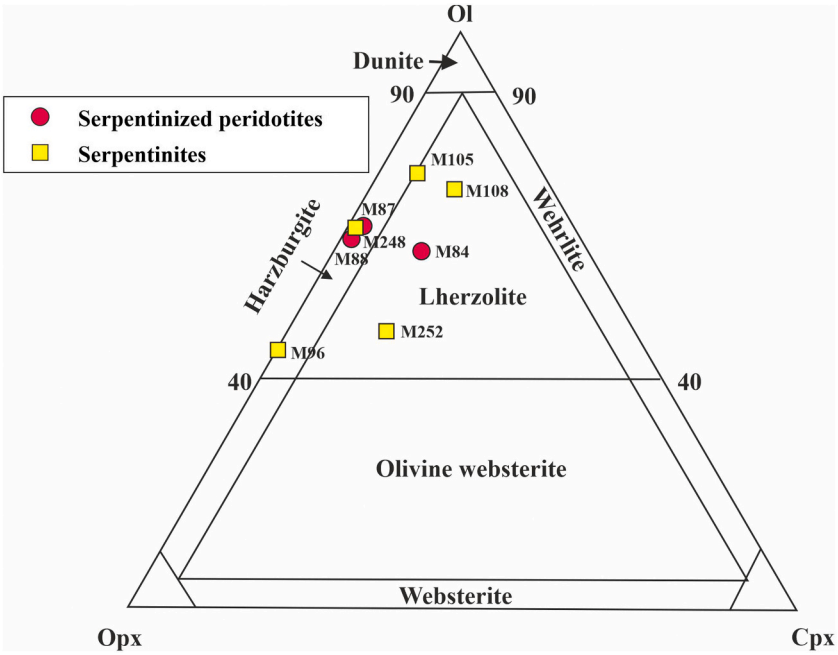

Fig. 8. Ol-Cpx-Opx normative composition of the studied ultramafic rocks (after Coleman, 1977).

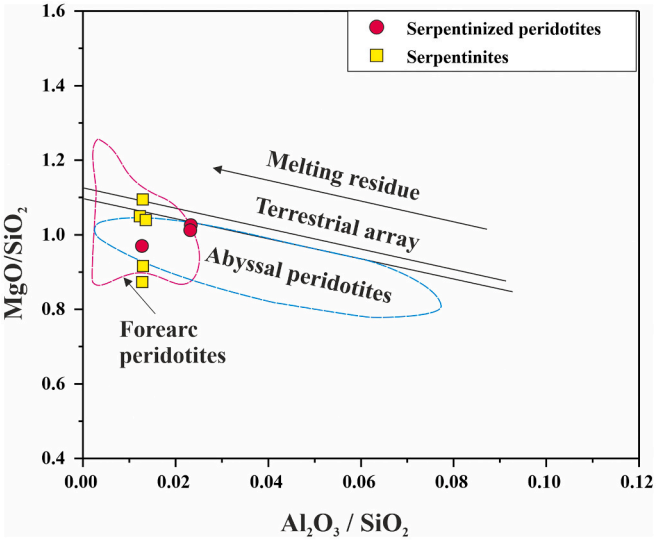

Fig. 9. MgO/SiO_2 vs. Al_2O_3/SiO_2 diagram for ultramafic rocks; terrestrial array is (after Jagoutz et al., 1979; Hart and Zindler, 1986), abyssal peridotite field (after Niu, 2004), field of fore-arc peridotites of South Sandwich and Izu-Bonin-Mariana (after Pearce et al., 2000; Parkinson and Pearce, 1998).

easily than in a back-arc setting (Stern, 2004). Ohara et al. (2002) concluded that Cr-Spinel from MOR and back-arc peridotites have Cr# <0.5, whereas Cr-spinel from fore-arc peridotite displays higher Cr#, up to 0.8, and Cr-spinel phenocrysts in boninite have Cr# of 0.7–0.9. Most of the serpentinized ultramafic rocks (M87 and M88 excepted) have Cr# (>0.6) and Mg# (<0.58) ranges similar to SSZ fore-arc peridotites. Even the high Al_2O_3 values in Cr-spinel of samples M87 and M88 mostly overlap the fore-arc peridotite range (Fig. 10d).

Some further indicators of fore-arc affinity can be found in whole-rock, olivine and clinopyroxene chemistry. The Al_2O_3/SiO_2 and MgO/SiO_2 ratios of the Wadi El-Mireiwa peridotite samples plot in the overlap region between strongly depleted abyssal peridotite and typical fore-arc peridotite (see Fig. 9). Excluding the exotic Mg-rich bands and metasomatized samples, olivine in Wadi El-Mireiwa peridotites has Mg# (0.86–0.92, average = 0.89) comparable to olivine in forearc peridotite (e.g., Coish and Gardner, 2004). The composition of clinopyroxene in the Wadi El-Mireiwa peridotite plots in the field of pyroxene crystallized from boninitic melts (Fig. 7b) and outside the fields of clinopyroxene from island arc tholeiite and MOR settings. This confirms the fore-arc setting, as boninite is a rock-type endemic to fore-arcs.

The earth's upper mantle commonly shows a large-scale heterogeneity in oxygen fugacity, generally attributed to the variable injection of oxidized materials into the otherwise more reducing upper mantle by oceanic subduction since the Neoproterozoic (Ballhaus et al., 1990). Many authors have noted that Cr-spinels from SSZ tectonic settings record more oxidizing conditions than those from MOR tectonic settings, resulting in strong correlation between fO_2 and Cr# (Parkinson and Pearce, 1998; Pearce et al., 2000). On the other hand, another group of authors argue that the Cr# of Cr-spinel does not correlate with fO_2 and that fore-arc peridotites record fO_2 similar to that of abyssal peridotites from the MOR setting (Birner et al., 2017). Recently, Cottrell et al. (2021) proposed that the upper mantle and derived magmas are most oxidized in arcs, followed by back-arcs and then by abyssal ridges. Thus, the oxidized nature of the Wadi El-Mireiwa ophiolitic peridotites ($\Delta \log fO_2$(FMQ) = +2.48 to +2.67) is consistent with a subduction-related rather than abyssal ridge tectonic setting. Additionally, the oxygen fugacity of Wadi El-Mireiwa serpentinized peridotites is similar to that reported for other Neoproterozoic fore-arc peridotites ($\Delta \log fO_2$(FMQ) = +0.88 to +4.50, Ahmed, 2013; +3.14 to +3.39, Maurice et al., 2021). On the other hand, fO_2 of the serpentinized peridotites rocks is lower than those recorded for the Neoproterozoic arc-associated Korab Kansi mafic-ultramafic layered intrusion ($\Delta \log fO_2$(FMQ) = +4.1 to +4.3, Khedr et al., 2020) of the south Eastern Desert of Egypt.

9.2. *Nature of the Wadi El-Mireiwa ultramafic rocks: Residual, cumulate or petrologic Moho?*

Depleted oceanic peridotites may be formed, in general, by several distinct processes; they may represent (1) mantle residues following removal of some degree of partial melt, (2) reaction products between wall-rock peridotite and infiltrating mafic melts, and (3) ultramafic

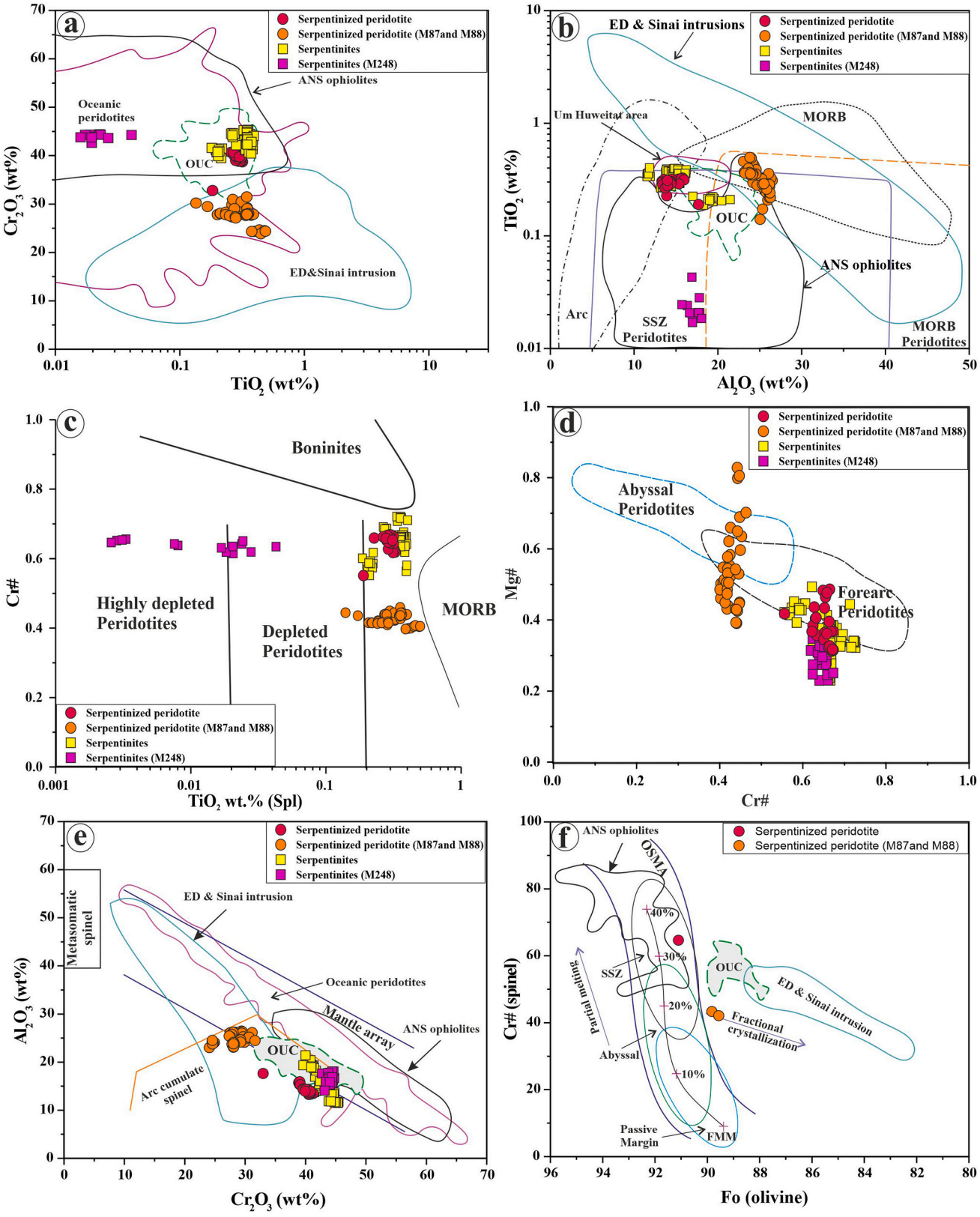

Fig. 10. Discrimination diagrams for tectonic setting based on Cr-spinel composition. (a) Cr_2O_3 vs. TiO_2 and (b) TiO_2 vs. Al_2O_3 (after Kamenetsky et al., 2001). Data sources: Um Huweitat cumulate (after Ali et al., 2020), ANS ophiolite, ED & Sinai intrusion, OUC (Oman ultramafic cumulate) and oceanic peridotite (after Maurice et al., 2021). (c) TiO_2 (wt%) vs. Cr# diagram for fresh spinel from different rock unit; fields are (after Dick and Bullen, 1984; Jan and Windley, 1990). (d) Mg# vs. Cr# of Cr-spinel (after Metcalf and Shervais, 2008). (e) Cr_2O_3 vs. Al_2O_3 diagram for the analyzed fresh spinel (after Franz and Wirth, 2000). Fields of ANS ophiolite, ED & Sinai intrusion, OUC (Oman ultramafic cumulate) and oceanic peridotite are after Maurice et al. (2021). (f) Fo content of the analyzed olivine vs. Cr# of the coexisting Cr-spinel from the studied serpentinized peridotites. OSMA refers to olivine-spinel mantle array (after Arai, 1994). Fields of ophiolitic ultramafic cumulate, ANS ophiolites and ED & Sinai intrusions are after Maurice et al. (2021).

cumulates formed in the lower oceanic crust by fractional crystallization processes. Various whole-rock and mineral chemistry indicators can help to distinguish among these categories. All the olivine in the Wadi El-Mireiwa serpentinized peridotite samples has low NiO contents, distinctly different from the olivine mantle array typical of residual peridotites (Fig. 5a). The hypothesis that the Wadi El-Mireiwa ultramafic rocks are products of melt-rock interaction is ruled out due to the absence of: (1) clinopyroxene resorption; (2) significant Ti contents in clinopyroxene (Fig. 7b) (e.g., Arai and Matsukage, 1996); or (3) LREE enrichment in the whole-rock compositions (Table S5). Hence, we favor the latter scenario, cumulate origin, for the Wadi El-Mireiwa peridotite rocks, and consider it in more detail in the following paragraphs.

Considering first the chemistry of relict olivine in the Wadi El-Mireiwa ultramafic rocks, the data are inconsistent with a residual mantle origin. Although the range of Fo contents (86–92) overlaps that of mantle peridotites (Fo 89–91), this is to be expected for crystals formed during early differentiation of a mantle-derived primitive magma. The MnO contents of the Wadi El-Mireiwa olivine and their relationship to Fo content are also unusual (Fig. 5b). They plot well above the OMA and define a trend with the opposite slope. They extend from the region of island arc ultramafic cumulates through the upper end of the ophiolitic ultramafic cumulates envelope into a previously little documented region at high Fo and high MnO (probably representing analyses that mix the normal regions with Mg-rich bands), ending at the compositions of the Mg-enriched bands discussed below. Setting aside for the moment the process that forms the MnO- and MgO-rich bands, the MnO content of the normal regions are, like the NiO data, consistent with a cumulate origin but not a residual origin.

Cr-spinel is a multi-component solid solution whose chemistry offers numerous petrogenetic clues. At Wadi El-Mireiwa, Cr-spinel in the serpentinized peridotite samples plots within the arc cumulate spinel field of a Cr_2O_3 vs. Al_2O_3 plot, while those in the serpentinite samples plot in ophiolitic ultramafic cumulate field (which overlaps the boundary between the arc cumulate and the mantle array fields, Fig. 10e). Most fresh Cr-spinel analyses from both ultramafic rock types at Wadi El-Mireiwa have high TiO_2 and Al_2O_3 contents, resembling spinel from the cumulate peridotite of the Um Huweitat ophiolite in the Eastern Desert (Ali et al., 2020) and plotting in the arc cumulate or OUC fields (Figs. 10b and e). Plotting the chemistry of olivine and co-existing Cr-spinel together using sample-by-sample averages (Fig. 10f), the serpentinized peridotite samples show some evidence of a fractional crystallization trend extending from a starting point on the olivine-spinel mantle array (OSMA) associated with SSZ residual peridotites. This is to be expected from a cumulate magmatic series that samples olivine and spinel crystals formed both in near-primary and somewhat evolved melts.

Clinopyroxene-based petrogenetic indicators tell a similar story. The Cr_2O_3 and Al_2O_3 contents (Fig. 7c) of clinopyroxene in the Wadi El-Mireiwa serpentinized peridotite overlap the fields of clinopyroxene from ANS ophiolites (which are mostly considered to represent fore-arc settings) and from island arc peridotites. The data do not plot in either of the regions of the Cr_2O_3 vs. Al_2O_3 diagram previously associated with mantle-crust transition zone peridotites, an area dominated by the products of melt-rock reaction. On an Al_2O_3 vs. Mg# diagram (Fig. 7d), the present clinopyroxene analyses define a negative correlation trend that mainly plots in the island arc peridotite field, which itself is entirely contained within the ANS ophiolite field (Fig. 7d). Similar negative correlations between Al_2O_3 and Mg# in clinopyroxene have been noted in ultramafic cumulates from the following ophiolites: Troodos (Hébert and Laurent, 1990), Mersin (Parlak et al., 1996), Oman (Koga et al., 2001), and both Ras Salatit (Gahlan et al., 2012) and Um Huweitat (Ali et al., 2020) in the Eastern Desert.

Although the mineral chemistry data suggests that the Wadi El-Mireiwa serpentinized peridotite and serpentinite largely represent ultramafic cumulates, serpentinite sample M248 from the ultramafic mass in the northwestern part of the study area appears to be distinct from the others in petrographic and chemical characteristics. Cr-spinel in sample M248 is represented by large, fractured crystals that contrast with the smaller, subhedral-to-euhedral Cr-spinel in the cumulate ultramafic samples. Moreover, Cr-spinel in M248 has high Mg#, high Cr#, and extremely low TiO_2 and Al_2O_3 contents that place these analyses in the field of Cr-spinel from depleted to highly depleted peridotite. The chemistry and texture of Cr-spinel in M248 most likely reflects a depletion event associated with the removal of a partial melt, as found in residual mantle rocks. This serpentinite sample therefore most likely is derived from the tectonite part of the ophiolite section.

Based on their petrographic, mineral chemical and whole-rock geochemical characteristics, and on their proximity to a large mass of ophiolitic clinopyroxenite, the majority of the Wadi El-Mireiwa serpentinized peridotites and serpentinite are best interpreted as magmatic rocks from the ultramafic cumulates at the base of the crustal section of a Neoproterozoic ANS ophiolite. Only one sample of serpentinite from the northwestern part of the study area likely represents the residual (mantle) part of this ophiolite. The serpentinized peridotite samples in the study area represent early-formed cumulate rocks, crystallized from magmas that would have been derived from near-primary melts extracted from mantle residues similar to the unique residual sample. Thus, the Wadi El-Mireiwa sequence captures both sides of the petrologic Moho of Neoproterozoic oceanic crust.

9.3. Origin of compositionally banded olivine

During our investigation of olivine in the Wadi El-Mireiwa serpentinized peridotite, we discovered notable intracrystalline chemical variations in the form of visible backscatter contrast due to differences in the major (Mg and Fe) and minor (Mn) element composition along a particular crystallographic direction, resulting in banded zoning (Figs. 3c and 6). Banded zoning of olivine has been documented from other localities and in different parts of the oceanic lithosphere. It is generally possible to distinguish in each case which is the main host olivine composition and which is the subordinate composition restricted to narrow bands. Fe-enriched bands were described in unaltered mantle-derived supra-subduction zone periodite in the Uenzaru peridotite complex (Hidaka metamorphic belt of central Hokkaido, Japan; Ando et al., 2001). Fe-enriched bands are also found in serpentinized meta-peridotite in the Mariana fore-arc (Conical and South Chamorro Seamounts; Murata et al., 2009). Both Fe-enriched bands in meta-dunite and Mg-enriched bands in meta-peridotite were found in the mantle section of the supra-subduction zone Leka Ophiolite Complex and Feragen ultramafic body of Norway (Plümper et al., 2012). In the present study, the banding is characterized by Mg-enriched stripes hosted by olivine with composition typical of oceanic peridotite. As far as we know, this is the first record of Mg-enriched (or, equivalently, Fe-depleted) banded zoning in olivine from any ultramafic rocks in the Arabian-Nubian Shield or from Neoproterozoic-aged rocks worldwide. In all these recorded cases, banded zoning in olivine is found in the fore-arc region of supra-subduction zone environments, either in the mantle or ultramafic cumulate sections of ophiolites.

Two general mechanisms have been proposed to explain crystallographically-oriented banded zoning in olivine. Both attribute the preferred orientation of the banding to the development of subgrain boundaries by amalgamation of dislocations during crystal-plastic deformation. The development and the motion of dislocations are both controlled by the active slip systems of deforming olivine crystals, and elastic strain energy is minimized when the dislocations become organized into planar arrays (e.g., Carter and Ave'Lallemant, 1970). Once such subgrain boundaries form, there are two hypotheses for how they might be expressed as chemical changes in the olivine: (1) solute atoms may be attracted to the distorted sites associated with dislocations and form an “atmosphere” around the dislocations (Cottrell, 1948); such a halo of elevated impurity concentration is often called a Cottrell atmosphere. When dislocations become organized into subgrain boundaries by dislocation creep, the Cottrell atmosphere would likewise assume the

form of oriented planes (Ando et al., 2001; Kitamura et al., 1986). Alternatively, (2) fluid infiltration into peridotite during antigorite serpentinization changes the composition of olivine that is in exchange equilibrium with coexisting phases, favoring increasing Mg/Fe, high MnO, and low NiO in olivine; the high-diffusivity channels formed by subgrain boundaries (Dohmen and Milke, 2010) allow rapid development of equilibrated olivine along the fast pathways, forming oriented and compositionally distinct bands. This mechanism requires that serpentinization accompanies or follows deformation (Murata et al., 2009; Plümper et al., 2012).

In the case of Mg-enriched (Fe-depleted) bands, as observed in the Wadi El-Mireiwa case, the Cottrell atmosphere mechanism can be ruled out as a cause. In a forsterite-rich olivine solid-solution, Fe^{2+} acts as the solute cation, so the expected solute concentration into a Cottrell atmosphere would produce Fe-enriched rather than Mg-enriched bands. Moreover, the Cottrell atmosphere is limited to about 1 nm from a dislocation, implying that excess solute concentrations observed at microprobe scale around an array of dislocations (i.e., subgrain boundary) would be unlikely to reach several percent via this mechanism (Plümper et al., 2012). Therefore, we are inclined to consider metasomatism by rapid diffusion along subgrain boundaries as the most plausible mechanism of Mg-enriched band formation. In cases where banded zoning in olivine has been assigned to diffusive equilibration with intergranular fluid, a specific connection to antigorite formation (Murata et al., 2009; Plümper et al., 2012) has been indicated by the presence of secondary olivine rims (overgrowing or replacing primary olivine) with Fo content similar to that of the bands (Murata et al., 2009). Raman spectroscopy of the Wadi El-Mireiwa serpentine shows that it is dominantly antigorite, suggesting that development of banded zoning in olivine could have been contemporaneous with and linked to antigorite formation. However, this mechanism would also produce Mg-enriched olivine rims, and these are not observed.

Further insight into the mechanism of olivine banding comes from considering the timing of band development relative to other events in the history of these rocks, including serpentinization, obduction, and contact metamorphism. With respect to serpentinization, development of banded zoning during initial serpentinization seems implausible for the following reasons. (1) When initial serpentinization occurs at high enough temperature to produce antigorite directly from olivine, magnetite does not form and in this case, given the strong partitioning of Mg into antigorite, mass balance requires that relict olivine have MgO contents lower than observed either between or in the bands (Evans, 2010). By contrast, low temperature retrogression of olivine in peridotite produces lizardite/chrysotile and magnetite (e.g., Evans, 2010), which may be subsequently modified by prograde metamorphism to antigorite plus disseminated magnetite, as observed at Wadi El-Mireiwa. (2) If indeed serpentinization occurred at low temperature in the lizardite stability field, then the rate of Fe-Mg interdiffusion, even along subgrain boundaries, would likely be too sluggish to produce Mg-rich stripes over 100 μm long (Dohmen and Milke, 2010). (3) Finally, as noted above, if the banded zoning developed during serpentinization, then olivine grain boundaries in direct contact with the intergranular fluid would also be chemically modified to Mg-rich, Mn-rich, Ni-poor compositions.

Development of olivine banding developed after serpentinization, e.g. due to contact metamorphism associated with granite intrusion, can also be ruled out. During post-serpentinization contact metamorphism, matrix serpentine surrounding olivine relics would also transform to olivine. Away from the contact zone, however, the ultramafic rocks remain fully serpentinized (Ahmed et al., 2012). The recrystallized metamorphic olivine in samples affected by granite intrusion is homogeneous and plainly distinct from the relict olivine that hosts the bands (Fig. 5a). The metamorphosed samples close to the granite intrusion also contain green spinel (Fig. 3g) and anthophyllite, but the samples with banded olivine lack these phases. Moreover, the samples bearing banded olivine are >3 km away from the nearest outcrop of biotite granite, which is greater than the common thickness of contact aureoles in ultramafic rocks (e.g., Arai, 1975; Nozaka and Shibata, 1995).

These considerations lead us to conclude that development of banded zoning in Wadi El-Mireiwa olivine in fact precedes serpentinization and persisted through the serpentinization process in the rare fresh olivine relics. This sequence of events implies that the banded zoning likely formed in a supra-subduction zone environment and predates obduction of the ophiolite. Olivine accommodates the deformation associated with plate tectonic motions by dislocation creep (Plümper et al., 2012). Kitamura et al. (1986) concluded that the assembly of olivine dislocations into subgrain boundaries requires high strain rates. By contrast, the Cottrell atmosphere is only thought to develop around slow-moving dislocations (Cottrell, 1948). In turn, formation of olivine banding at Wadi El-Mireiwa via Fe-Mg exchange along oriented subgrain boundaries implies that the strain rate in this Neoproterozoic supra-subduction zone spreading system was rapid, which in the Phanerozoic is characteristic of fore-arc settings. The cumulate nature of the Wadi El-Mireiwa peridotite further implies that the high strain-rate dislocation creep regime encompassed not only the mantle wedge but also the ultramafic part of the lower crust.

9.4. Implications for lithospheric metasomatism in a Neoproterozoic supra-subduction zone setting

We attribute the formation of banded olivine in Wadi El-Mireiwa serpentinized peridotites to the infiltration of a high-Mg/Fe^{2+} metasomatic fluid during high strain-rate deformation. Reaction to form high-Mg olivine implies that the ratio of Mg^{2+} activity to Fe^{2+} activity in the fluid was correspondingly elevated; this might reflect a high Mg content in the solute budget of the fluid, a highly oxidizing state that maintained most of the Fe in the fluid in the Fe^{3+} state, or both. Here we discuss additional evidence for cryptic metasomatism (change in chemistry without change in modal mineralogy) in these rocks. Specifically, the presence of reversely zoned Cr-spinel suggests shifts in whole-rock composition. Chromian spinels are widely used as petrogenetic indicators for detecting the source characteristics, evolution, and tectonic setting of fresh and altered mantle peridotites (Barnes and Roeder, 2001; Dick and Bullen, 1984; Irvine, 1967) and for detecting hydrothermal alteration and metamorphism via distinctive zoning patterns (Arai and Akizawa, 2014; Klein-BenDavid et al., 2011; Satsukawa et al., 2015). Normal zoning in Cr-spinel, characterized by Al- and Mg-rich cores and Cr- and Fe-rich rims, is the most common type. Normal zoning in Cr-spinel has been reported in most ophiolites (Ahmed et al., 2016), layered mafic intrusions (Evans and Frost, 1975), komatiites (Barnes, 2000) and metamorphosed ultramafic massifs (Colás et al., 2014). It can develop during melting and fractional crystallization processes (Dick and Bullen, 1984) but may also reflect metamorphism that selectively removes Al and Mg to form ferritchromite/magnetite rims (Barnes, 2000).

Reverse zoning, by contrast, is defined by Fe- and Cr-rich cores surrounded by Al- and Mg-rich rims. This type of Cr-spinel zoning has been reported by several authors (e.g., Ahmed et al., 2008; Gamal El Dien et al., 2019; Sinton, 1977; Yang and Seccombe, 1993). Although reverse zoning in Cr-spinel has been investigated in some mineralogical, geochemical and experimental studies, the origin of this feature remains a matter of debate. Proposed mechanisms for development of reverse zoning in Cr-spinel grains include (1) melt-rock interaction, (2) exchange with co-existing solid silicates, (3) deformation, and (4) exchange with metasomatic fluids.

(1) Clearly, when the rims of Cr-spinel crystals come into contact with melts more primitive than those they previously equilibrated with, the resulting reaction may generate reverse distribution of elements, preserving a spinel core of different composition if the reaction does not go to completion. This mechanism has been invoked to explain Cr-spinel with sharp

boundaries between Cr-rich cores and Al-rich rims in arc volcanic rocks and greenstone belts (e.g., Allan et al., 1989). In some cases, this model is supported by the coexistence, in seamount lavas and tholeiitic basalts, of reversely zoned spinel with homogeneous spinel inclusions in olivine, shielded from reaction with mixed magma (e.g., Allan et al., 1989).

(2) Elemental exchange between Cr-spinel grains and coexisting silicate minerals may occur by diffusion in the absence of melt, given sufficient time at high but subsolidus temperatures (Bai et al., 2018; Lehmann, 1983; Sinton, 1977; Yang and Seccombe, 1993). This interpretation was reported for coexisting spinel and enstatite in the Red Mountain Alpine-type mafic-ultramafic complex on the South Island of New Zealand (Sinton, 1977), where continuous reaction led to the enrichment of enstatite in Cr and Fe, forming complementary Al- and Mg-rich rims on spinel grains. A similar interpretation was offered for reversely zoned Cr-spinel grains in the Gabbro Akarem mafic-ultramafic complex in Egypt (Ahmed et al., 2008) and the Yanmenguan mafic-ultramafic complex in the North China Craton (Bai et al., 2018).

(3) Deformation, surprisingly, affects not only the microstructure of Cr-spinel but also its chemistry (Ando et al., 2001; Ozawa, 1989). Deviatoric stress drives Cr-Al interdiffusion in the spinel structure, yielding dipolar zoning of Al and Cr in elongated spinel grains in deformed peridotites (Ozawa, 1989). This mechanism operates in the diffusion creep regime (Coble, 1963). It is possible for Cr-spinel to deform by diffusion creep while coexisting olivine is deforming by dislocation creep.

(4) Finally, heterogeneity of Cr-spinel — including reverse zoning — may reflect interaction with hydrothermal or metasomatic fluids in the upper mantle (Ahmed et al., 2016; Arai and Akizawa, 2014). Such metasomatic fluids may move slowly through peridotites by grain-boundary permeability, allowing cryptic metasomatism over long timescales, or rapidly by crack propagation. The resulting zoning patterns depend on the chemistry of the fluid, the intensive parameters of the system, and the fluid/rock ratio.

In our case study at Wadi El-Mireiwa, high-resolution compositional line scans (by EDS) across selected Cr-spinel grains display a clear reverse distribution of MgO and FeO contents from the inner core to the outer core, while the Al_2O_3 and Cr_2O_3 contents are nearly constant (Fig. 11). This pattern exists inside the ferritchromite rim, which sharply truncates the gradual zoning of the core region. Melt-rock interaction seems implausible as a mechanism in this case: geochemical analyses reveal a highly depleted nature for the Wadi El-Mireiwa peridotites, with low whole-rock Al_2O_3, high MgO, and most rare earth and incompatible trace elements very low (many below our detection limit). Subsolidus exchange with silicate minerals is also excluded, since exchange reactions that deplete Cr-spinel in Fe would result in fayalitic olivine, which we do not observe. There is no halo of Fe-enriched serpentine minerals around Cr-spinel grains. The deformation-induced mechanism is not consistent with the observations of reverse zoning of Cr-spinel at Wadi El-Mireiwa. These rocks have massive texture with no marked foliation, their Cr-spinel does not show any elongation or lineation, and the zoning is not dipolar.

Hence, by elimination and for further reasons, we prefer fluid-rock interaction (metasomatism) as the mechanism to develop reverse zoning in Cr-spinel grains in serpentinized peridotite at Wadi El-Mireiwa. Mg-rich rims of Cr spinel grains may be formed by the infiltration of the same high-Mg/Fe^{2+} metasomatic fluids that drove formation of Mg-rich bands in coexisting olivine. A marked intragranular transport of divalent ions (Fe-Mg) may occur without significant motion of trivalent ions (Cr-Al-Fe^{+3}), as divalent ion diffusion rates in the spinel structure are several orders of magnitude faster than those for trivalent ions (Ahmed et al., 2008). Such a distinction between the behavior of divalent and trivalent cations is indeed observed (Fig. 11).

The calculated oxygen fugacity [$\Delta \log fO_2$(FMQ)] values vary from +2.48 to +2.67 for the unmetasomatized Cr-spinel-olivine pairs and from +3.75 to +4.53 for the metasomatized parts of Cr-spinel if they equilibrated with the Mg-rich olivine bands. This indicates that the interaction of metasomatic fluids with peridotite resulted in an increase in the oxygen fugacity values of the metasomatized parts of the rock, implying that the Neoproterozoic subduction zone fluids were oxidized, which may by itself explain the elevation of Mg relative to Fe^{2+} in the spinel.

10. Conclusions

1. The Wadi El-Mireiwa serpentinized peridotite and serpentinite represent, respectively, cumulate and residual ultramafic members of a piece of Neoproterozoic oceanic lithosphere, obducted by thrusting above metasedimentary rocks and an island arc assemblage during closure of the Mozambique Ocean.
2. The geochemical and mineral chemical characteristics of the Wadi El-Mireiwa ultramafic rocks indicate that some of the serpentinite samples are residual upper mantle tectonites, whereas the serpentinized peridotite samples are cumulate lower crustal rocks. In the field, the serpentinized peridotite coexists with extensive outcrops of clinopyroxenite, supporting a cumulate origin for these samples, because cumulate pyroxenites are present as large belts that extend for several kilometers (e.g. DeBari and Coleman, 1989). The highly depleted nature of the residual samples points to a supra-subduction zone origin, most likely at a fore-arc spreading center.
3. Mg-rich bands in olivine grains in the Wadi El-Mireiwa serpentinized peridotite are the first record of such a texture in Neoproterozoic ophiolitic rocks. Although the Cottrell atmosphere hypothesis may explain Fe-enriched bands in olivine, here we prefer a model whereby subgrain boundaries that formed by olivine dislocation creep in a high-strain-rate flow can operate as high-diffusivity channels for Mg ions from high-Mg/Fe^{2+} metasomatic fluids in the intergranular medium, resulting in the formation of oriented Mg-enriched bands in the olivine crystals. Our analysis of the likely timing of formation of banded zoning in olivine suggests an early process during spreading of oceanic lithosphere, preceding serpentinization.
4. Reverse zoning of Mg and Fe in the cores of Cr-spinel grains in serpentinized peridotite are likely metasomatic in origin and may have formed in response to infiltration of the same high-Mg/Fe^{2+} fluid that supported the formation of Mg-rich bands in olivine.
5. The oxygen fugacity [$\Delta \log fO_2$(FMQ)] values recorded by the fresh (fO_2 = +2.48 to +2.67) and metasomatized (fO_2 = +3.75 to +4.53) parts of the Wadi El-Mireiwa serpentinized peridotites indicate that Neoproterozoic subduction zone metasomatic fluids were oxidized and increased the oxygen fugacity of the metasomatized parts of the serpentinized peridotites.
6. The formation of banded zoning in olivine of Wadi El Mireiwa cumulate serpentinized peridotite implies that dislocation creep produced by crystal-plastic deformation can extend to the ultramafic cumulate part of the oceanic crust and is not restricted to the mantle section of the fore-arc oceanic crust. Moreover, this mechanism implies a high strain rate for this Neoproterozoic case, analogous to the high strain rates observed in Phanerozoic fore-arc spreading events. Banded zoning has now been recorded in both Phanerozoic and Neoproterozoic fore-arc settings, suggesting that this texture may be a specific fingerprint for the fore-arc tectonic environment.

Supplementary data to this article can be found online at https://doi.org/10.1016/j.lithos.2022.106894.

Declaration of Competing Interest

The authors declare that they have no known competing financial

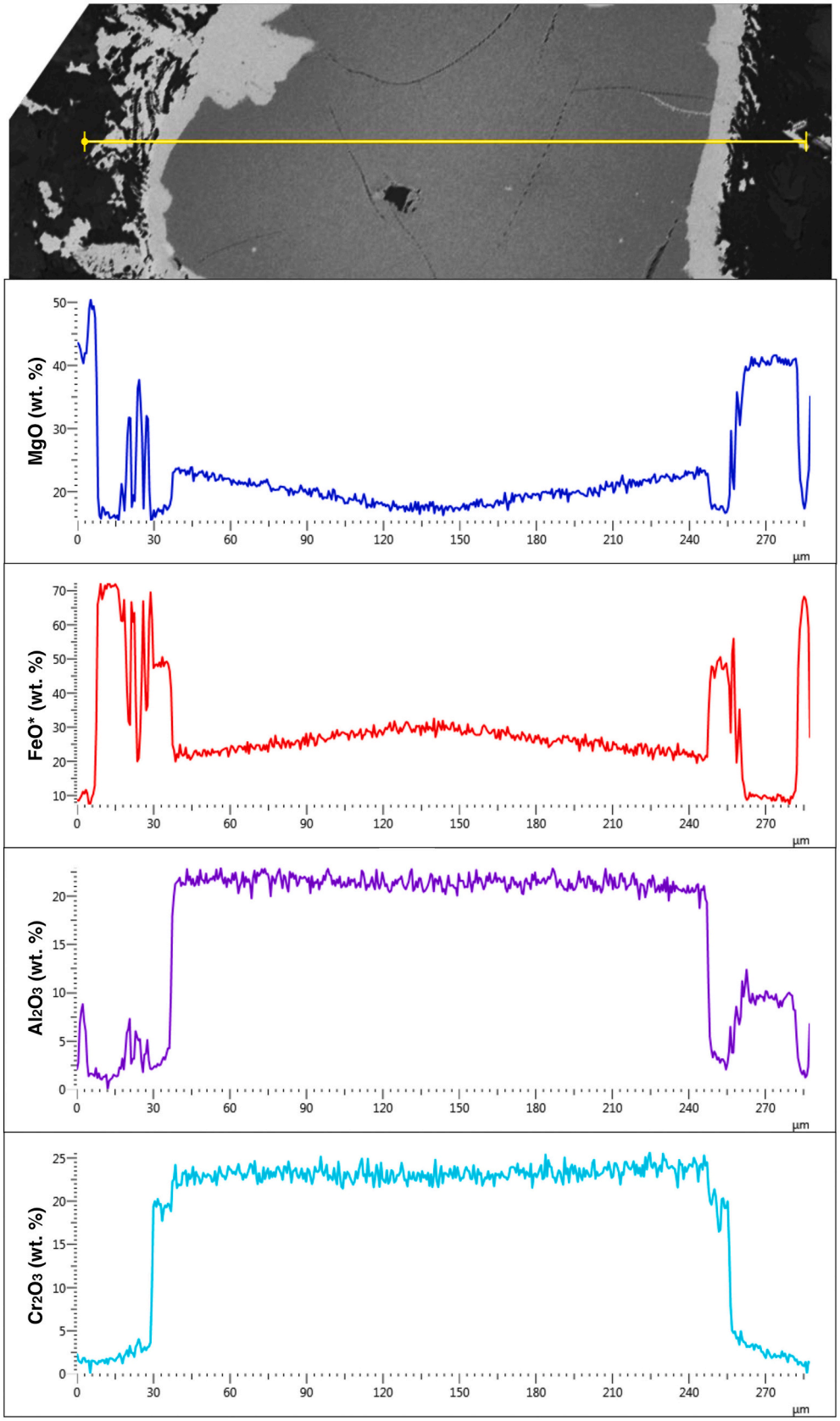

Fig. 11. High-resolution, high-precision X-ray line scan for Cr-spinel showing the distribution of MgO, FeO, Al_2O_3 and Cr_2O_3.

interests or personal relationships that could have appeared to influence the work reported in this paper.

Acknowledgements

Comments by two anonymous reviewers were helpful in improving the manuscript. We thank Dr. Greg Shellnutt (Editor) for careful editorial handling. PDA acknowledges support from the US National Science Foundation, award 1947616.

References

Abd El-Rahman, Y., Polat, A., Dilek, Y., Fryer, B.J., El-Sharkawy, M., Sakran, S., 2009. Geochemistry and tectonic evolution of the Neoproterozoic incipient arc-forearc crust in the Fawakhir area, Central Eastern Desert of Egypt. Precambrian Res. 175, 116–134.
Abdel-Karim, A.M., Ali, S., Helmy, H.M., El-Shafei, S.A., 2016. Fore-arc setting of the Gerf ophiolite, Eastern Desert, Egypt: evidence from mineral chemistry and geochemistry of ultramafites. Lithos 263, 52–65.
Ahmed, A.H., 2013. Highly depleted harzburgite-dunite-chromitite complexes from the Neoproterozoic ophiolite, south Eastern Desert. Precambrian Res. 233, 173–192.
Ahmed, A.H., Helmy, H.M., Arai, S., Yoshikawa, M., 2008. Magmatic unmixing in spinel from late Precambrian concentrically-zoned mafic-ultramafic intrusions, Eastern Desert, Egypt. Lithos 104, 85–98.
Ahmed, A.H., Gharib, M., Arai, S., 2012. Characterization of the thermally metamorphosed mantle-crust transition zone of the Neoproterozoic ophiolite at Gebel Mudarjaj, south Eastern Desert, Egypt. Lithos 142, 67–83.
Ahmed, A.H., Moghazi, A.K., Moufti, M.R., Dawood, Y.H., Ali, K.A., 2016. Nature of the lithospheric mantle beneath the Arabian Shield and genesis of Al-spinel micropods: evidence from the mantle xenoliths of Harrat Kishb, Western Saudi Arabia. Lithos 240–243, 119–139.
Ali, R.A.M., Pitcairn, I.K., Maurice, A.E., Azer, M.K., Bakhit, B.R., Shahien, M.G., 2020. Petrology and geochemistry of ophiolitic ultramafic rocks and chromitites across the Eastern Desert of Egypt: Insights into the composition and nature of a Neoproterozoic mantle and implication for the evolution of SSZ system. Precambrian Res. 337, 105565.
Allahyari, K., Saccani, E., Rahimzadeh, B., Zeda, O., 2014. Mineral chemistry and petrology of highly magnesian ultramafic cumulates from the Sarve-Abad (Sawlava) ophiolites (Kurdistan, NW Iran): new evidence for boninitic magmatism in intra-oceanic forearc setting in the Neo-Tethys between Arabia and Iran. J. Asian Earth Sci. 79, 312–328.
Allan, J.F., Batiza, R., Perfit, M.R., Fornari, D.J., Sack, R.O., 1989. Petrology of lavas from the Lamont seamount chain and adjacent East Pacific rise, 10° N. J. Petrol. 30, 1245–1298.
Ando, J., Shibata, Y., Okajima, Y., Kanagawa, K., Furusho, M., Tomioka, N., 2001. Striped iron zoning of olivine induced by dislocation creep in deformed peridotites. Nature 414 (6866), 893–895.
Arai, S., 1975. Contact metamorphosed dunite-harzburgite complex in the Chugoku district, western Japan. Contrib. Mineral. Petrol. 52 (1), 1–16.
Arai, S., 1994. Characterization of spinel peridotites by olivine-spinel compositional relationships: review and interpretation. Chem. Geol. 113 (3–4), 191–204.
Arai, S., Akizawa, N., 2014. Precipitation and dissolution of chromite by hydrothermal solutions in the Oman ophiolite: new behavior of Cr and chromite. Am. Mineral. 99, 28–34.
Arai, S., Matsukage, K., 1996. Petrology of gabbro-troctolite-peridotite complex from Hess deep, equatorial Pacific: Implications for mantle-melt interaction within the oceanic lithosphere. In: In Proceedings-Ocean Drilling Program Scientific Results. National Science Foundation, pp. 135–156.
Azer, M.K., Stern, R.J., 2007. Neoproterozoic (835–720 Ma) serpentinites in the Eastern Desert, Egypt: Fragments of fore-arc mantle. J. Geol. 115, 457–472.
Bai, Y., Su, B.X., Xiao, Y., Lenaz, D., Asamoah Sakyi, P., Liang, Z., Yang, S.H., 2018. Origin of reverse zoned Cr-spinels from the Paleoproterozoic Yanmenguan mafic–ultramafic complex in the North China Craton. Minerals 8 (2), 62.
Ballhaus, C., Berry, R.F., Green, D.H., 1990. Oxygen fugacity controls in the Earth's upper mantle. Nature 348, 437–440.
Barnes, S.J., 2000. Chromite in komatiites, II. Modification during greenschist to mid-amphibolite facies metamorphism. J. Petrol. 41, 387–409.
Barnes, S.J., Roeder, P.L., 2001. The range of spinel compositions in terrestrial mafic and ultramafic rocks. J. Petrol. 42 (12), 2279–2302.
Basta, F.F., Maurice, A.E., Bakhit, B.R., Ali, K.A., Manton, W.I., 2011. Neoproterozoic contaminated MORB of Wadi Ghadir Ophiolite, NE Africa: geochemical and Nd and Sr isotopic constraints. J. Afr. Earth Sci. 59, 227–242.
Beccaluva, L., Macciotta, G., Piccardo, G.B., Zeda, O., 1989. Clinopyroxene composition of ophiolite basalts as petrogenetic indicator. Chem. Geol. 77, 165–182.
Birner, S.K., Warren, J.M., Cottrell, E., Davis, F.A., Kelley, K.A., Falloon, T.J., 2017. Forearc peridotites from Tonga record heterogeneous oxidation of the mantle following subduction initiation. J. Petrol. 58 (9), 1755–1780.
Boutier, A., Brovarone, A.V., Martinez, I., Sissmann, O., Mana, S., 2021. High-pressure serpentinization and abiotic methane formation in metaperidotite from the Appalachian subduction, northern Vermont. Lithos 396, 106190.
Carter, N.L., Ave'Lallemant, H.G., 1970. High temperature flow of dunite and peridotite. Geol. Soc. Am. Bull. 81, 2181–2202.
Clarke, E., De Hoog, J.C.M., Kirstein, L.A., Harvey, J., Debret, B., 2020. Metamorphic olivine records external fluid infiltration during serpentinite dehydration. Geochem. Perspect. Lett. 16, 25–29.
Coble, R.L., 1963. A model for boundary diffusion-controlled creep in polycrystalline materials. J. Appl. Phys. 34 (6), 1679–1682.
Coish, R.A., Gardner, P., 2004. Suprasubduction-zone peridotite in the northern USA Appalachians: evidence from mineral composition. Mineral. Mag. 68, 699–708.
Colás, V., González-Jiménez, J.M., Griffin, W.L., Fanlo, I., Gervilla, F., O'Reilly, S.Y., 2014. Fingerprints of metamorphism in chromite: New insights from minor and trace elements. Chem. Geol. 389, 137–152.
Coleman, R.G., 1977. Ophiolites: Ancient Oceanic Lithosphere?: Berlin/Heidelberg. Springer, Germany, p. 229.
Cottrell, A.H., 1948. In Report on the Strength of Solids. The Physical Society, London p, pp. 30–36.
Cottrell, E., Birner, S., Brounce, M., Davis, F.A., Waters, L.E., Kelley, K.A., 2021. Oxygen fugacity across tectonic settings. In: Moretti, R., Neuville, D.R. (Eds.), Magma Redox Geochemistry: AGU Geophysical Monograph Series, 266, pp. 33–61.
DeBari, S.M., Coleman, R.G., 1989. Examination of the deep levels of an island arc: evidence from the Tonsina ultramafic-mafic assemblage, Tonsina, Alaska. J. Geophys. Res. Solid Earth 94 (B4), 4373–4391.
Dick, H.J., Bullen, T., 1984. Chromian spinel as a petrogenetic indicator in abyssal and alpine-type peridotites and spatially associated lavas. Contrib. Mineral. Petrol. 86 (1), 54–76.
Dohmen, R., Milke, R., 2010. Diffusion in polycrystalline materials: grain boundaries, mathematical models, and experimental data. Rev. Mineral. Geochem. 72 (1), 921–970.
El-Gharbawi, R.I.A., 1988. Petrological and Petrochemical Studies of Igneous and Metamorphic Rocks of Gabal Mudargag Area, South Eastern Desert, Egypt. PhD thesis. Faculty of Science, Ain Shams University, Cairo, Egypt.
El-Sharkawy, M.A., El-Bayoumi, R., 1979. The ophiolites of Wadi Ghadir area, Eastern Desert, Egypt. Ann. Geol. Surv. Egypt 9, 125–135.
Evans, B.W., 2010. Lizardite versus antigorite serpentinite: magnetite, hydrogen, and life (?). Geology 38 (10), 879–882.
Evans, B.W., Frost, B.R., 1975. Chrome-spinel in progressive metamorphism—a preliminary analysis. Acta Geochim. 39, 959–972.
Franz, L., Wirth, R., 2000. Spinel inclusions in olivine of peridotite xenoliths from TUBAF seamount (Bismarck Archipelago/Papua New Guinea): evidence for the thermal and tectonic evolution of the oceanic lithosphere. Contrib. Mineral. Petrol. 140 (3), 283–295.
Gahlan, H.A., Arai, S., Abu El-Ela, F.F., Tamura, A., 2012. Origin of wehrlite cumulates in the Moho transition zone of the Neoproterozoic Ras Salatit ophiolite, Central Eastern Desert, Egypt: crustal wehrlites with typical mantle Characteristics. Contrib. Mineral. Petrol. 163, 225–241.
Gahlan, H.A., Azer, M.K., Khalil, A.E.S., 2015. The Neoproterozoic Abu Dahr ophiolite, South Eastern Desert, Egypt: petrological characteristics and tectonomagmatic evolution. Mineral. Petrol. 109, 611–630.
Gamal El Dien, H., Arai, S., Doucet, L.S., Li, Z.X., Kil, Y., Fougerouse, D., Hamdy, M., 2019. Cr-spinel records metasomatism not petrogenesis of mantle rocks. Nat. Commun. 10 (1), 1–12.
Hart, S.R., Zindler, A., 1986. In search of a bulk-Earth composition. Chem. Geol. 57 (3–4), 247–267.
Hébert, R., Laurent, R., 1989. Mineral chemistry of ultramafic and mafic plutonic rocks of the Appalachian ophiolites, Québec, Canada. Chem. Geol. 77 (3–4), 265–285.
Hébert, R., Laurent, R., 1990. Mineral chemistry of the plutonic section of the Troodos ophiolite: New constraints for genesis of arcrelated ophiolites. In: Malpas, J., Moores, E., Panayiotou, A., Xenophontos, C. (Eds.), Ophiolites–Oceanic Crustal Analogues. Proceedings of Troodos Ophiolite symposium 1987. Nicosia, Cyprus Geological Survey, pp. 149–163.
Irvine, T.N., 1967. Chromian spinel as a petrogenetic indicator: part 2. Petrologic applications. Can. J. Earth Sci. 4 (1), 71–103.
Jagoutz, E., Palme, H., Baddenhausen, H., Blum, K., Cendales, M., Dreibus, Wänke, H., 1979. The abundances of major, minor and trace elements in the earth's mantle as derived from primitive ultramafic nodules. In: In Lunar and Planetary Science Conference Proceedings, 10, pp. 2031–2050.
Jan, M.Q., Windley, B.F., 1990. Chromian spinel-silicate chemistry in ultramafic rocks of the Jijal complex, Northwest Pakistan. J. Petrol. 31 (3), 667–715.
Kamenetsky, V.S., Crawford, A.J., Meffre, S., 2001. Factors controlling chemistry of magmatic spinel: an empirical study of associated olivine, Cr-spinel and melt inclusions from primitive rocks. J. Petrol. 42, 655–671.
Kempf, E.D., Hermann, J., 2018. Hydrogen incorporation and retention in metamorphic olivine during subduction: Implications for the deep water cycle. Geology 46 (6), 571–574.
Khedr, M.Z., El-Awady, A., Arai, S., Hauzenberger, C., Tamura, A., Stern, R.J., Morishita, T., 2020. Petrogenesis of the ~740 Korab Kansi mafic-ultramafic intrusion, South Eastern Desert of Egypt: evidence of Ti-rich ferropicritic magmatism. Gondwana Res. 82, 48–72.
Kitamura, M., Matsuda, H., Morimoto, N., 1986. Direct observation of the Cottrell atmosphere in olivine. Pro. Japan Acad. Series B 62 (5), 149–152.
Klein-BenDavid, O., Pettke, T., Kessel, R., 2011. Chromium mobility in hydrous fluids at upper mantle conditions. Lithos 125, 122–130.
Koga, K.T., Kelemen, P.B., Shimizu, N., 2001. Petrogenesis of the crust-mantle transition zone and the origin of lower crustal wehrlite in the Oman ophiolite. Geochem. Geophys. Geosyst. 2 (9).
Lehmann, J., 1983. Diffusion between olivine and spinel: Application to geothermometry. Earth Planet. Sci. Lett. 64, 123–138.

Maurice, A.E., Azer, M.K., Asimow, P.D., Basta, F.F., Helmy, H.M., Shibata, T., 2021. The Kabr El-Bonaya peridotites, Southeastern Sinai, Egypt: petrology, geochemistry, and metamorphism of Neoproterozoic arc ultramafic cumulates. Am. J. Sci. 321 (10), 1445–1496.
Metcalf, R.V., Shervais, J.W., 2008. Suprasubduction-zone ophiolites: is there really an ophiolite conundrum? In: Wright, J.E., Shervais, J.W. (Eds.), Ophiolites, Arcs, and Batholiths: A Tribute to Cliff Hopson, 438. Geological Society of America Special Paper, pp. 191–222.
Morimoto, N., Fabries, J., Ferguson, A.K., Ginzburg, I.V., Ross, M., Seifert, F.A., Zussman, J., 1988. Nomenclature of pyroxenes. Min. Mag. 52, 535–550.
Murata, K., Maekawa, H., Yokose, H., Yamamoto, K., Fujioka, K., Ishii, T., Chiba, H., Wada, Y., 2009. Significance of serpentinization of wedge mantle peridotites beneath Mariana forearc, Western Pacific. Geosphere 5, 90–104.
Niu, Y., 2004. Bulk-rock major and trace element compositions of abyssal peridotites: Implications for mantle melting, melt extraction and post-melting processes beneath mid-ocean ridges. J. Petrol. 45, 2423–2458.
Nozaka, T., 2010. A note on compositional variation of olivine and pyroxene in thermally metamorphosed ultramafic complexes from SW Japan. Okayama University, Earth Sci. Rep. 17, 1–5.
Nozaka, T., Shibata, T., 1995. Mineral paragenesis in thermally metamorphosed serpentinites, Ohsa-yama, Okayama Prefecture. Okayama Univ. Earth Sci. Rep. 2 (1), 1–12.
Ohara, Y., Stern, R.J., Ishii, T., Yurimoto, H., Yamazaki, T., 2002. Peridotites from the Mariana Trough: first look at the mantle beneath an active back-arc basin. Contrib. Mineral. Petrol. 143 (1), 1–18.
Ozawa, K., 1989. Stress-induced Al-Cr zoning of spinel in deformed peridotites. Nature 338, 141–144.
Parkinson, I.J., Pearce, J.A., 1998. Peridotites from the Izu Bonin-Mariana forearc (ODP Leg 125): evidence for mantle melting and melt-mantle interaction in a supra-subduction zone setting. J. Petrol. 39, 1577–1618.
Parlak, O., Delaloye, M., Bíngöl, E., 1996. Mineral chemistry of ultramafic and mafic cumulates as an indicator of the arc-related origin of the Mersin ophiolite (southern Turkey). Geol. Rundsch. 85 (4), 647–661.
Pearce, J.A., Barker, P.F., Edwards, S.J., Parkinson, I.J., Leat, P.T., 2000. Geochemistry and tectonic significance of peridotites from the South Sandwich arc-basin system, South Atlantic. Contrib. Mineral. Petrol. 139, 36–53.
Petriglieri, J.R., Salvioli-Mariani, E., Mantovani, L., Tribaudino, M., Lottici, P.P., Laporte-Magoni, C., Bersani, D., 2015. Micro-Raman mapping of the polymorphs of serpentine. J. Raman Spectrosc. 46 (10), 953–958.
Plümper, O., King, H.E., Vollmer, C., Ramasse, Q., Jung, H., Austrheim, H., 2012. The legacy of crystal-plastic deformation in olivine: high-diffusivity pathways during serpentinization. Contrib. Mineral. Petrol. 163 (4), 701–724.
Saccani, E., Tassinari, R., 2015. The role of MORB and SSZ magma-types in the formation of Jurassic ultramafic cumulates in the Mirdita ophiolites (Albania) as deduced from chromian spinel and olivine chemistry. Ofioliti 40 (1).
Satsukawa, T., Piazolo, S., González-Jiménez, J., Colás, V., Griffin, W.L., O'Reilly, S.Y., Gervilla, F., Fanlo, I., Kerestedjian, T.N., 2015. Fluid-present deformation aids chemical modification of chromite: insights from chromites from Golyamo Kamenyane, SE Bulgaria. Lithos 228–229, 78–89.
Shahien, M.G., Azer, M.K., Asimow, P.D., 2021. Neoproterozoic Ophiolites of the Arabian-Nubian Shield. In: The Geology of the Arabian-Nubian Shield. Springer, Cham, pp. 297–330.
Sinton, J.M., 1977. Equilibration history of the Basel alpine-type peridotite, Red Mountain, New Zealand. J. Petrol. 18, 216–246.
Stern, R.J., 2004. Subduction initiation: spontaneous and induced. Earth Planet. Sci. Lett. 226, 275–292.
Stevens, R.E., 1944. Composition of some chromites of the Western Hemisphere. Am. Mineral. 29 (1–2), 1–34.
Takahashi, E., Uto, K., Schilling, J.G., 1987. Primary magma compositions and Mg/Fe ratios of their mantle residues along mid-Atlantic ridge 29°N to 73°N. In: Technical Report, v. A9, Institute for Study of the Earth's Interior, Okayama University Series, pp. 1–14.
Trommsdorff, V., Evans, B.W., 1972. Progressive metamorphism of antigorite schist in the Bergell tonalite aureole (Italy). Am. J. Sci. 272 (5), 423–437.
Yang, K., Seccombe, P.K., 1993. Chemical variation of chromite in the ultramafic cumulates of the Great Serpentinite Belt, Upper Bingara to Doonba, New South Wales, Australia. Can. Mineral. 31, 75–87.
Zimmer, M., Kröner, A., Jochum, K.P., Reischmann, T., Todt, W., 1995. The Gabal Gerf complex: a Precambrian N-MORB ophiolite in the Nubian Shield, NE Africa. Chem. Geol. 123, 29–51.
Zoheir, B., Abd El-Rahman, Y., Kusky, T., Xiong, F., 2022. New SIMS zircon U-Pb ages and oxygen isotope data for ophiolite nappes in the Eastern Desert of Egypt: Implications for Gondwana assembly. Gondwana Res. 105, 450–467.